Nonlinear optics in 2D materials: from classical to quantum

Liuxin Gu[1], You Zhou[1,2*]

[1]Department of Materials Science and Engineering, University of Maryland, College Park, MD 20742, USA

[2]Maryland Quantum Materials Center, College Park, Maryland 20742, USA

*To whom correspondence should be addressed: youzhou@umd.edu

Abstract. Nonlinear optics has long been a cornerstone of modern photonic technology, enabling a wide array of applications, from frequency conversion to the generation of ultrafast light pulses. Recent breakthroughs in two-dimensional (2D) materials have opened a frontier in this field, offering new opportunities for both classical and quantum nonlinear optics. These atomically thin materials exhibit strong light-matter interactions and large nonlinear responses, thanks to their tunable lattice symmetries, strong resonance effects, and highly engineerable band structures. In this paper, we explore the potential that 2D materials bring to nonlinear optics, covering topics from classical nonlinear optics to nonlinearities at the few-photon level. We delve into how these materials enable possibilities, such as symmetry control, phase matching, and integration into photonic circuits. The fusion of 2D materials with nonlinear optics provides insights into the fundamental behaviors of elementary excitations—such as electrons, excitons, and photons—in low-dimensional systems and has the potential to transform the landscape of next-generation photonic and quantum technologies.

1. Overview

The field of nonlinear optics examines the behaviors of light in media where the polarization density is not directly proportional to the electric field of the light. Light entering such a nonlinear medium can alter the refractive index, generate new frequencies, or modify its own path through effects like self-focusing.[1,2] In addition, such nonlinearities can mediate interactions among photons, which become strong at high light intensities—typically requiring lasers to generate.

The study of nonlinear optics has significantly advanced our fundamental understanding of light-matter interactions under a strong optical field, enabling breakthroughs in nonlinear spectroscopy[3], frequency conversion[4], and the creation of non-equilibrium states in materials[5–7]. It has also propelled fields such as attosecond science[8], allowing scientists to probe the dynamics of atoms, molecules, and solids on ultrafast timescales shorter than one femtosecond. Meanwhile, nonlinear optics has also greatly expanded our capabilities to generate, manipulate, and detect light, forming the cornerstone of many modern optical technologies, such as ultrafast lasers[9,10], supercontinuum generation[11–13], and optical modulators[14–16], with broad applications in industries including telecommunications[17–20], spectroscopy[3,21,22], and bio-medical imaging[23,24].

Meanwhile, an emerging frontier in nonlinear optics explores the intersection with quantum optics, where both fields converge to enable groundbreaking quantum technologies[25] (**Fig. 1**). On the one hand, nonlinear optics plays a critical role in quantum optics by facilitating the development of key technologies, such as the generation of entangled photon pairs through spontaneous parametric down-conversion (SPDC)[26], which forms the foundation of quantum communication systems and quantum networks[27,28]. On the other hand, remarkable progress in quantum optics has significantly reduced the power requirements for nonlinear optical processes, reaching the single-photon level in meticulously engineered quantum systems[25,29]. Achieving such strong nonlinearity at the individual photon level allows for quantum control of light fields, opening avenues for unique applications such as single-photon switches, all-optical deterministic quantum logic, and highly efficient optical transistors[30–32].

Central to the science and technology of classical and quantum nonlinear optics is the challenge in developing materials with strong optical nonlinearity, higher efficiency, improved scalability, integration compatibility, and stability. In particular, materials with high nonlinear coefficients would enable more efficient photon interactions, naturally reducing the power required to achieve nonlinear effects and making these processes more accessible and scalable for applications. Another major challenge is the integration of nonlinear optical materials and devices with linear optics platforms, such as photonic integrated circuits and metasurfaces[33,34]. This difficulty lies in achieving compatible growth and fabrication processes for nonlinear materials, such as lithium niobate ($LiNbO_3$), on substrates with distinct physical and chemical properties[4,35–37].

In this context, recent studies of two-dimensional (2D) materials, such as transition metal dichalcogenides (TMDs)[38], graphene[39], and black phosphorus[40], present promising opportunities for overcoming many challenges faced by traditional materials[41,42]. These atomically thin materials exhibit extraordinary properties, including readily controllable lattice symmetry, large exciton binding energies, sizable interactions among quasiparticles, and tunable band gaps—all of which contribute to stronger light-matter interactions[43–45] and enhanced optical nonlinearity[46–50]. Additionally, 2D materials offer unprecedented flexibility in designing lattice and electronic structures by forming van der Waals heterostructures[41,51]. Moreover, the heterostructures can be readily integrated onto various photonic platforms, including photonic integrated circuits and

metasurfaces[16,52–54]. As such, the study of nonlinear optical processes in 2D materials not only provides physical insights into electron, exciton, and phonon dynamics but also opens new avenues for creating more efficient and compact optical devices for applications in classical and quantum optical technologies.

In this paper, we review the fundamental principles of nonlinear optics in 2D materials and explore their potential applications in both classical and quantum regimes. We begin by providing a brief overview of the mechanisms behind nonlinear optics, emphasizing the key properties of 2D materials that make them particularly intriguing for nonlinear optics. Next, we delve into various nonlinear optical processes in 2D materials, starting with second-order and third-order nonlinearities and concluding with higher-order effects. We then focus on nonlinear optical phenomena at low photon levels, approaching the quantum regime. Finally, we offer an outlook on the field, discussing both the prospects and challenges in advancing the science and technology of nonlinear and quantum optics with 2D materials.

2. Introduction

2.2 Nonlinear optics mechanisms

The nonlinear optical effect occurs when the volume polarization $P(t)$ of a material does not linearly depend on the applied optical field $E(t)$. In particular, the optical response can be described by the following equation in the time domain:

$$P(t) = \epsilon_0\chi^{(1)}E(t) + \epsilon_0\chi^{(2)}E^2(t) + \epsilon_0\chi^{(3)}E^3(t) + \cdots\cdots\cdots$$

where ϵ_0 is the permittivity in free space, $\chi^{(1)}$ is the materials linear susceptibility, and $\chi^{(n)}$refers to the *n*th order (n>1) nonlinear susceptibility. As seen from Equation (1), the strength of nonlinear optical processes substantially increases with stronger optical fields, and it is precisely these higher-order processes that enable the generation of different frequencies. More generally, equation (1) shall be expressed in the frequency domain and the $\chi^{(n)}(\omega)$ characterize the *n*th order (n>1) nonlinear susceptibility at frequency ω. Typically, materials with large nonlinear susceptibility are favorable due to their stronger nonlinear response.

Notably, $\chi^{(n)}(\omega)$ can be complex, allowing for the classification of nonlinear processes as either parametric or non-parametric. In parametric processes, only the real part of the susceptibility is relevant, meaning energy exchange occurs solely among interacting photons, with total photon energy conserved. The initial and final quantum states of the material remain the same, without any photon absorption, or any exchange of momentum or angular momentum between the optical field. Since the material's quantum state remains unchanged, parametric processes can occur on extremely short timescales by the uncertainty principle ($\Delta t \approx \hbar/2\Delta E$). Examples of such include frequency conversion, such as second harmonic generation (SHG), via a virtual state.

The nonparametric process occurs when the material has a complex susceptibility with a nonzero imaginary component. In such nonlinear processes, energy exchange occurs not only between the photons but also between light and the material itself. As a result, nonparametric processes involve energy transfer between the ground state and excited state, typically exhibiting longer lifetimes. Examples of nonparametric processes include saturable absorption (SA), two-photon absorption (TPA), and stimulated Raman scattering (SRS).

Phase matching is important in all nonlinear optical processes and is required to achieve efficient nonlinear frequency conversion. For nonparametric processes, phase matching is automatically satisfied, which is not true for parametric processes. For example, in the case of frequency doubling, two photons, each with a wavevector $\boldsymbol{k}_1$, creates another photon with a wavevector k_2 at the harmonic frequency. Although the total momentum is conserved, there could be a finite difference in their wavevectors:

$$\Delta \boldsymbol{k} = \boldsymbol{k}_2 - 2\boldsymbol{k}_1$$

This is due to the chromatic dispersion of materials. Ideally, the phase-matching conditions $\Delta k = 0$ needs to be satisfied to achieve efficient frequency conversion. This means that all the electric dipoles in the system are in phase, and the field emitted by each dipole can add up constructively in a forward direction. In this case, the harmonic field would grow linearly with the propagation length and with a quadratic increase in the harmonic intensity.

Achieving the exact phase matching can be difficult due to the material's dispersion. With a nonzero $\Delta \boldsymbol{k}$, the harmonic field oscillates sinusoidally along the propagation length, with a periodicity of $\frac{2\pi}{\Delta \boldsymbol{k}}$. The coherence length $l_c \sim \frac{\pi}{\Delta \boldsymbol{k}}$, represents the maximum distance over which the harmonic field generated in a medium can add constructively to the harmonic generated earlier in the medium. A finite coherence length limits the efficiency of frequency conversion. Various techniques have been developed to minimize the phase mismatch, including birefringent phase matching, critical phase matching, and quasi-phase matching[55].

2.3 2D materials and opportunities for nonlinear optics

Over the past decade, two-dimensional (2D) materials have emerged as an exciting platform for photonic and optoelectronic applications[56]. The family of 2D materials encompasses diverse materials with distinct structural, electronic, and optical properties. These materials can crystallize in structures with various symmetries, and exhibit all sorts of electronic properties, including those of metals, semimetals, semiconductors, insulators, and superconductors[57,58]. Importantly, individual layers can be stacked into van der Waals heterostructures in an almost arbitrary fashion, offering unprecedented flexibility in engineering their electronic and optical responses[41,51]. Given these features, it is no surprise that great efforts are ongoing in exploring the physics and application of 2D materials in linear optics.

Alongside their impact on linear optics, 2D materials possess several attributes that make them intriguing for nonlinear optics[59–61]. For instance, crystal symmetry plays a key role in even-order nonlinear processes, which can be controlled in 2D heterostructures[62]. In particular, the family of group VI transition metal dichalcogenides (TMDs) (MX_2, M = Mo, W; X = S, Se, Te) are semiconductors that exhibit strong optical response with their bandgap in the visible and near-infrared regime[63–65]. These materials can exist in multiple crystal structures, such as hexagonal 2H, rhombohedral 3R, or trigonal 1T' phases, each with distinct symmetries and corresponding nonlinear optical responses[66,67] (Fig. 2b). Furthermore, they can be stacked with varying twist angles and material compositions to engineer different types of symmetry-breaking and nonlinear responses[68] (Fig. 2b).

In addition, 2D materials often exhibit large nonlinear susceptibilities due to their reduced dimensionality and electronic structures, which enhance their light-matter interactions. The reduced dimensionality leads to the weak screening of Coulomb interactions, resulting in a strong

response of various quasiparticles to external light fields[44]. This is also true of strong interactions between optical excitations, which can mediate photon-photon interactions. In fact, several types of resonances, including surface plasmon polaritons[69–71], phonon polaritons[71,72], and excitons polariton[73–75], have been shown to exhibit strong linear and nonlinear optical responses in 2D material families[76,77].

In TMDs, for instance, weak screening and the relatively heavy carrier effective mass result in tightly bound excitons with large oscillator strengths[78,79]. This not only leads to a strong linear optical response— excitonic reflectance or absorption stronger than the band edge—but also enhances nonlinear effects, resonantly enhanced by excitons[80,81](Fig. 2c). Exciton resonances in 2D materials can be tuned via methods such as electrostatic gating[82,83] and strain[84,85], potentially enabling rapid *in-situ* control of nonlinear susceptibilities[86,87]. Additionally, these 2D semiconductors exhibit valley-dependent optical selection rules, where circularly polarized light couples to a specific valley[88–90]. Such valley degeneracy can be broken by external magnetic fields or polarized optical pumping, leading to chiral light-matter coupling and potentially even chiral nonlinearity[91,92].

In terms of phase matching, the atomic thickness of 2D materials—significantly thinner than the wavelength of light—results in negligible dispersive dephasing during light propagation (Fig. 2d). As a result, 2D materials automatically satisfy phase-matching conditions[66,93,94], making them desirable for nonlinear optical applications[95]. Finally, the van der Waals heterostructures of 2D materials can be integrated onto virtually any substrate without requiring lattice matching, making them promising for integration with photonic circuits and metasurfaces[52,96] (Fig. 2e). Techniques are being developed to create such structures with atomic precision, at the back end-of-line processing stage.

Overall, the ability to control symmetry, leverage quantum confinement[97], harness strong resonance effects, and exploit ultrafast carrier dynamics and tunability[98], combined with ease of integration, makes 2D materials exceptionally well-suited for applications in nonlinear optics, including frequency conversion, optical modulation[14,99], and the development of compact, high-performance photonic devices[100] as well as quantum technology[101,102].

3. Second Order Nonlinearity

Second-order nonlinearity is when the induced polarization is proportional to the square of the electric field. This nonlinearity is described by the second-order susceptibility tensor $\chi^{(2)}$, and it gives rise to several important processes in nonlinear optics, including second harmonic generation (SHG), sum-frequency generation (SFG), and difference-frequency generation (DFG). The symmetry of the materials plays a crucial role in these second-order processes. In particular, they only occur in materials with non-centrosymmetric geometry[103], since the inversion symmetry dictates that $\chi^{(2)}$must vanish in centrosymmetric materials.

SHG, SFG, and DFG all involve frequency conversion via the 2nd order nonlinearity. In the SHG process, when a wave with frequency ω is incident on a medium with a finite $\chi^{(2)}$, the nonlinear polarization generates two terms, one at zero frequency and another at the second harmonic frequency 2ω. The conversion into the second harmonic can be highly efficient, allowing for the almost entire conversion from ω into the second harmonic under optimal conditions. In

contrast, the SFG and DFG process occurs when two waves with different frequencies (ω_1, ω_2) interact to generate a third wave at a frequency ω_3, where $\omega_3 = \omega_1 + \omega_2$ in SFG and $\omega_3 = \omega_1 - \omega_2$ in DFG, respectively. The DFG process is a particularly useful nonlinear process for generating tunable light sources and entangled photon pairs, which will be discussed in more detail later. Crucially, the phase matching and energy conservation have to be satisfied in all these nonlinear optical processes. Due to the dispersion of conventional nonlinear media materials, there is often a trade-off between the phase-matching bandwidth and conversion efficiency.

3.1 Second Order Nonlinear effects in 2D materials

3.1.1 Symmetry control. Since second-order nonlinearity requires broken inversion symmetry, only specific types and stacking configurations of 2D materials can produce this nonlinear effect. Notably, monolayer transition metal dichalcogenides (TMDs) without any inversion symmetry have been explored extensively for these effects[67,104]. Intriguingly as the number of layers increases, different stacking configurations lead to different nonlinear behaviors. For example, in the 2H phase of TMDs, inversion symmetry is broken in materials with an odd number of layers but is restored when there is an even number of layers. This results in finite second-harmonic generation (SHG) in odd layers and zero SHG in even layers[105](Fig. 4a).. In contrast, in the 3R phase (rhombohedral stacking), each monolayer is stacked in the same orientation, maintaining a non-centrosymmetric structure regardless of the number of layers. Consequently, in 3R stacking, the SHG intensity increases quadratically with the number of layers when the layer thickness is smaller than the coherence length, as the contributions from each layer add up constructively[66,106,107](Fig. 4c). This observation points to the possibility of controlling the second-order nonlinear response by artificially stacking such layers rather than using naturally formed layers, which favors 2H stacking due to its thermodynamic stability.

3.1.2 Resonant enhancement. In 2D materials, the strong resonance effect, such as excitons, can substantially affect their nonlinear response. In particular, the value of χ^2 and SHG efficiency can be greatly enhanced when the SHG energy is close to any exciton resonance, due to the dramatically enhanced light-matter interaction[80,108]. As expected, the strongest SHG intensity occurs at the 1s exciton state, which can be explained by the proximity of the 1s exciton energy to intermediate virtual transition levels. In one study[80] (Fig. 3a), an enhanced SHG efficiency by a factor of 3 was observed in monolayer WSe_2 when scanning the two-photon laser energy across the excitonic spectrum. Since both the oscillator strength and energies of excitons can be tuned by doping[109], the resonantly enhanced SHG efficiency can be also modulated by gating. For instance, a four-fold reduction in the SHG intensity can be observed when electrostatically doping monolayer WSe_2[110].

3.1.3 Electrical control of symmetry breaking. Interestingly an electric field can be used to break the inversion symmetry and induce a finite $\chi^{(2)}$ in materials without structural inversion symmetry breaking. For instance, when a 2H-stacked bilayer MoS_2 with inversion symmetry is under an electric field, the SHG intensity can reach a value comparable to that in monolayer[111]. This is attributed to the interlayer exciton transition, where the Coulomb-bound electrons and holes are spatially separated across two layers. With sa stronger electric field, the electronic layer polarization becomes more prominent, which leads to an increase in the value of $\chi^{(2)}$. Importantly, interlayer excitons exhibit a static out-of-plane electric dipole such that their energies can be tuned

by applied electric field via the Stark effect[82,112] (Fig. 3b,c) . This means Stark effect can also tune the resonant energies at which exciton enhancement of $\chi^{(2)}$ is the most prominent. In fact, the SHG intensity increases quadratically with the applied electric field, reaching a maximum enhancement by a factor of 25 at the interlayer exciton resonant energy of 0.17 MV/cm compared to the SHG intensity at zero electric field (Fig. 3d) [111]. Similar interlayer exciton-enhancement of SHG has also been observed in 2H bilayer WSe_2[113] and 3R MoS_2[66]. In addition to forming dipolar interlayer excitons, an electric field can also break symmetry by polarizing doped carriers in structurally symmetric 2D materials, thereby inducing a finite SHG signal. For example, in a doped 2H-WSe_2 bilayer under an electric field, free carriers, such as electrons or holes, can become layer-polarized, which results in a 40-fold enhancement in net SHG[114] (Fig. 3e-f).

3.1.4 Nonlinear coefficient and conversion efficiency.

Interestingly it has been noted that monolayer and few-layer TMDs exhibit rather large nonlinear optical susceptibilities comparable with conventional nonlinear materials. For instance, in monolayers of MoS_2, WS_2, WSe_2, and $MoSe_2$, $\chi^{(2)}$ can reach the order of ~nm/V, even significantly higher than conventional nonlinear crystals, where $\chi^{(2)}$ is typically around pm/V[115]. However, the reported susceptibility in TMDCs varies widely, ranging from several pm/V to even hundreds of nm/V[60]. Several factors contribute to the variation in the reported values of susceptibilities, such as the materials quality, sample fabrication methods (e.g., exfoliated versus chemical vapor deposition (CVD) grown flakes)[116], local strain[117,118] and doping[119]Furthermore, the nonlinear susceptibilities are highly wavelength-dependent and can be enhanced near optical resonances of materials, such as exciton energies, when nonparametric processes can become important. Therefore, it is crucial to consider these details when examining the nonlinear properties of TMDs.

Despite the relatively large nonlinear coefficient, the SHG efficiency is usually low, due to the atomically thin nature of 2D materials. Classically the intensity of SHG can be expressed as: $I_{2\omega} \propto I_0^2 l^2 sinc^2(\frac{\Delta k \cdot l}{2})^1$, where l is propagation length. For instance, in MoS_2 [120], the efficiency is ~10^{-7} at the second harmonic wavelength of 810 nm with Ti: Sapphire pump peak intensity of 10 GW cm^{-2}. In WSe_2 [110] at 1470 nm excitation with a pump peak intensity of 24 GW cm^{-2}, the estimated conversion efficiency for the on-resonance SHG (A exciton) is ~10^{-10}. This is in comparison with conventional NLO materials, such as thin film (600 nm) $LiNbO_3$, where the SHG conversion can reach a few percentages under similar pump peak intensity[121]. Such low efficiency is because SHG only occurs within the atomically thin layer in 2D materials, while in conventional materials, all the signals within the coherence length can constructively interfere to produce much stronger signal, even when the susceptibility is smaller[122,123]. To achieve optimal efficiency, one may stack multiple layers together but needs to consider the chromatic dispersion, and the TMD thickness shall match the coherence length, ensuring constructive interference[93].

3.1.5 SHG as a probe. Because the $\chi^{(2)}$ tensor reflects the crystally symmetry and the wavelength at which $\chi^{(2)}$ is enhanced is highly dependent on the materials, SHG is an effective method for identifying the crystallographic orientation of materials, with material selectivity even in heterostructures. In these measurements, a linearly polarized laser is incident on the sample, and the SHG signal intensity is detected with the same linear polarization. By rotating the in-plane polarization, one can map out the SHG intensity and determine the crystallographic orientation. For instance, since in monolayer TMDs with D_{3h} symmetry, the second-order nonlinear

susceptibility follows $\chi^2_{xxx} = -\chi^2_{xyy} = -\chi^2_{yyx} = -\chi^2_{yxy}$. where x, y corresponds to the armchair and zigzag direction[105]. When the input laser polarization is parallel to the analyzer (the SHG signal polarization), the SHG intensity collected can be expressed as $I_{||} = I_0 \cos^2(3\phi)$. For the perpendicular case, the SHG intensity is: $I_{\perp} = I_0 \sin^2(3\phi)$, where ϕ is the angle between the input laser polarization and the armchair x direction[62]. As a result, the in-plane SHG intensity exhibits a six-fold symmetric pattern as the polarization is rotated in-plane (Fig. 4b).

3.1.6 OPA and OPO

The DFG process is widely used for generating coherent tunable light sources in processes such as optical parametric amplification (OPA) and optical parametric oscillation (OPO). During this process, the energy of the higher energy pump photon $h\omega_1$ transfer into the two lower energy states, creating an additional lower-energy photon, referred to as the signal, at ω_2, and generating a third photon, called the idler, at ω_3. With a strong pump, this process amplifies the intensity of the signal light in an OPA process. OPO, on the other hand, occurs when such a nonlinear system is placed inside an optical cavity, which is resonant with at least one of the signal and idler waves. This cavity feedback creates a continuous generation of signal and idler photons, turning the OPO into a coherent light source with high photon conversion efficiency.

Since OPA and OPO allow the amplification of light at frequencies within the transparency range of the nonlinear medium, provided that phase-matching conditions are met, they are of great technological impact creating tunable coherent light sources that can span a broad spectral range and are widely used in quantum optics to generate squeezed coherent states of light is to extend their operation bandwidth[124,125]. Currently, the bandwidth of OPO and OPA is largely constrained by the phase-matching requirements, such as the reliance on birefringence phase-matching[126,127]. 2D materials with atomic thickness could offer interesting opportunities for relaxing and engineering the phase-matching conditions if they can have large susceptibilities[94]. Early results demonstrate that in monolayer $MoSe_2$, the seed photon energy can be tuned over a broad range from 0.83 eV to 1.21 eV with a fixed pump energy (3.11 eV) while the idler photon energy changes from 2.28 eV to 1.90 eV[128] (Fig. 4d). This tuning range reported is limited by the tuning laser range, while it is still large compared to certain nonlinear materials, such as submicrometric periodically poled $KTiOPO_4$ (PPKTP) with a ~1.073 to 1.11 eV tuning range[127], but smaller than Ti: Sapphire waveguide amplifier with a tuning range of ~1.13 to 1.91 eV[129]. In addition, by inserting a monolayer of 1T'-$MoTe_2$ or 2H-$MoTe_2$ film into the cavity of a femtosecond OPO, effective modulation of the pulse spectral width as well as a compression of pulse duration by a factor of 20 is observed[130].

Similar to SHG, the OPA and OPO efficiency can be also enhanced by increasing the number of layers in R-stacked multilayers, pointing to the new possibility of symmetry control[107]. These early results demonstrate the promise of 2D materials for OPA applications, for instance, by selecting materials with different bandgaps, one may be able to achieve a larger transparency window and tuning range[131].

3.1.7 Spontaneous Parametric Down Conversion (SPDC)

Another important DFG process is the spontaneous parametric down-conversion (SPDC), where a pump photon spontaneously decays into two lower-energy photons: the signal and the idler. This process obeys both energy conservation as $\omega_1 = \omega_2 + \omega_3$ and momentum conservation $k_1 = k_2 + k_3$ but occurs without external control. The signal and idler photons, produced as a pair,

can be entangled in various fashions, such as polarization, energy-time, and position-momentum entanglement. For instance, in a so-called type-II SCPD process, the signal and idler photons have orthogonal polarizations whose wavefunction can be described as a polarization-entangled Bell state[132–134]. As such, the SPDC process is critical for creating entangled photon pairs and single photons for experiments in quantum optics and quantum information science[135].

As phase matching is relaxed in ultrathin materials, it could enable SPDC over a wide spectral range. For instance, the generation of correlated photons through the SPDC process has been recently reported in a 2D material, niobium oxide dichloride ($NbOCl_2$)[136]. The photon statistics is characterized by the second-order correlation function $g^{(2)}(\tau)$ as a function of delay time τ, which is defined as $g^{(2)}(\tau) = \frac{<N_s(t)N_i(t+\tau)>}{<N_s(t)><N_i(t+\tau)>}$, $N_{s,i}$ refers to the signal or idler photon numbers registered at the detectors. When pumping thin $NbOCl_2$ flakes with a 3mW 404nm CW laser, a two-photon correlation peak $g^{(2)}(0)$ of ~25 is observed, indicating a temporal correlation between the generated photons. Due to the low crystal symmetry in $NbOCl_2$, the efficiency of this process is highly dependent on the input polarization, and it is difficult to define a polarization-entangled state that is favorable for certain quantum communication schemes.

In contrast, a well-defined polarization entanglement can be generated using 2D materials with a three-fold in-plane rotational symmetry, such as TMDs[137]. As shown in Fig. 5, when pumping with linear polarization direction along *x* or *y* (here *x* is along zigzag and *y* is along armchair direction), one can create two maximally entangled Bell states which can be expressed as $\phi^- = \frac{1}{\sqrt{2}}\left(|HH>_{s,i} - |VV>_{s,i}\right)$ for *x*-polarization pump and $\psi^+ = \frac{1}{\sqrt{2}}\left(|HV>_{s,i} + |VH>_{s,i}\right)$ for the *y*-polarization pump (Figs. 5a-c). By varying the pumping polarization angle, the generated state can be a superposition of the above two Bell states. Thanks to the symmetry in TMD, varying the pump polarization does not change the photon generation efficiency[137,138], which is a highly desirable feature for applications.

In addition, entangled photon pairs in the telecom regime (~1550nm) can be generated using multilayer MoS_2[137]. Experiments show a coincidence-to-accidental ratio (CAR) of 8.9±5.5 (where CAR = $g^{(2)}(0) - 1$), with low PL background noise under 5.6 mW of 788 nm excitation[139] . However, compared with conventional nonlinear crystals such as BBO or PPLN(Periodically Poled $LiNbO_3$ waveguide) and nanoscale metasurface[140–142] , the SPDC efficiency is still low due to the ultra-short propagation length[143,144]. For any practical applications, further improvement in overall efficiency needs to be investigated. In addition, integrating 2D materials with metasurfaces may also be an intriguing aspect for developing other forms of entanglement.

4. Third Order Nonlinearity

4.1 Parametric process

The third-order nonlinear process deals with $\chi^{(3)}$nonlinearity term and is more common than second-order nonlinearity since it doesn't require broken inversion symmetry. Two important nonlinear optical processes can occur when the applied optical field is monochromatic: third-harmonic generation (THG) and the Kerr effect. In particular, with an input field of $E(t) = E\cos\omega t$, the 3rd-order nonlinear dipole moment is given by:

$$P^{(3)}(t) = \epsilon_0 \chi^{(3)} E^3(t) = \frac{1}{4}\epsilon_0 \chi^{(3)} E^3 \cos 3\omega t + \frac{3}{4}\epsilon_0 \chi^{(3)} E^3 \cos \omega t$$

The first term describes the THG process where three photons of frequency ω interact to generate one photon with a frequency of 3ω. The second term, proportional to $E(t)$, represents a change in the refractive index of the medium, experienced by the ω photons. This intensity-dependent refractive index change is also known as Kerr effect, and its effect on the refractive index can be described as:

$$n = n_0 + n_2 I$$

where n_0 is the linear refractive index, I is the intensity of the incident beam ($\sim E^2$), and n_2 is the Kerr constant related to the real part of $\chi^{(3)}$:

$$n_2 = \frac{3}{4n_0^2 \epsilon_0 c} Real(\chi^{(3)}).$$

The Kerr effect results in the modification of light propagation. For instance, when light with non-uniform intensity propagates in a material with a positive Kerr constant n_2, the regions of higher intensity experience a larger change in the refractive index. This causes the beam to bend toward the higher-intensity regions, making it self-focus.

4.1.2 Kerr and THG

The third-order nonlinear process exhibits ultrafast response in the femtosecond regime, and this has motivated the exploration of ultrafast all-optical switching and signal generation. Since the change of the refractive index can induce the phase change, 2D materials with large Kerr nonlinearity can be applied to novel optical phase modulation. For instance, the Kerr constant reported in 2D materials exhibits a large value at the scale of ~10^{-11} m^2/W[131] (for monolayer transition metal dichalcogenides). Particularly, graphene also owns a large range of the Kerr constant from ~10^{-11}- 10^{-15} m^2/W in telecommunication banda[145]. These are all several orders higher than that in bulk materials in silicon[146](10^{-18} m^2/W) or silicon nitride[147](10^{-19} m^2/W). In 2D semiconductors such as TMDs, optical pumping can induce significant changes in the resonance energies of optical excitations, such as excitons. Such resonance-enhanced Kerr effects will be discussed in more detail in the later part of this review.

In addition to the Kerr effect, frequency conversion is a crucial basement for application in short wavelength laser generation, spectroscopy[3] as well as imaging[23]. High-order harmonic conversion is less efficient than lower-order nonlinear frequency conversion, thus, requiring higher pump power. It is reported that in monolayer MoS_2 the THG efficiency is ~ 10^{-10} at the wavelength of 520nm[148]. This value scales with the number of layers in MoS_2(2H).

4.1.3 FWM

More generally, when the input field is polychromatic, the 3rd order nonlinear response can also produce frequency conversion, often called four waves mixing (FWM). For instance, in non-degenerate four wave mixing (NDFWM) where $\omega_1 \neq \omega_2 \neq \omega_3$, three waves interact in the media to generate a fourth frequency wave, at relationships such as $\omega_4 = \omega_1 + \omega_2 + \omega_3$, $\omega_4 = \omega_1 + \omega_2 - \omega_3$, $\omega_4 = \omega_1 + \omega_3 - \omega_2$, $\omega_4 = \omega_2 + \omega_3 - \omega_1$; and. In degenerate four-wave mixing (DFWM), there are three input field at the same frequency $\omega_1 = \omega_2 = \omega_3$, but with two strong beams coming from opposite directions and a weaker signal wave. A fourth wave is created

at the same frequency ($\omega_4 = 2\omega - \omega$) but with a phase conjugate to the signal wave. Overall, similar to 2nd order linear processes, FWM is also highly useful for developing OPA and for wavelength conversion applications.

Four-wave mixing has been utilized as a spectroscopic technique to study exciton dynamics[149]. Specifically, in an optical two-dimensional Fourier-transform spectroscopy[150,151], three ultrafast pulses $\mathcal{E}_a^*, \mathcal{E}_b, \mathcal{E}_c$, usually in the femtosecond regime, incident onto the sample to create a fourth FWM signal with different time delayers (Fig. 6a). The generated FWM and the excited three beams satisfy the phase-matching relationship as $\boldsymbol{k_{FWM} = -k_a + k_b + k_c}$. By measuring the FWM intensity as a function of the time delay (τ_a, τ_b), one can quantify the dephasing and relaxation dynamics of optical excitations, which is typically challenging to do from linear spectroscopy. Specifically, the first pulse creates a coherent superposition of the ground state and excited state, which evolves freely within the first-time delay τ_a, subject to the inhomogeneous broadening. The second and third reverse the state and phase accumulation during τ_c, which cancels out the dephasing due to inhomogeneous broadening and produces a photon echo.

The 2D Fourier transform spectra are often presented by Fourier transforming the measured spectrum $S(\tau_a, \tau_b, \tau_c)$ into $S(h\omega_A, \tau_b, h\omega_C)$, from which one can not only measure the absorption and emission, but also the homogeneous vs. inhomogeneous broadening[152](Fig.6b). This has been proved helpful for studying various optical excitations in 2D materials, such as excitons in TMDs with large homogeneous broadening. Furthermore, one can probe the role of exciton-exciton[152,153], exciton-phonon[152,154] and charge-exciton interactions[155], all of which contribute to linewidth broadening. Moreover, by using different circularly polarized light in the pulse sequence, one can access the valley dynamics, for example, measuring valley decoherence, from such measurements[156] (Fig. 6c-d).

4.2 Nonparametric process

In addition to the parametric process, there are nonparametric third-order nonlinear effects such as saturable absorption (SA) and two-photon absorption (TPA). SA occurs when a high-intensity laser reduces the absorption coefficient and increases the transmission of the material. SA effect is mainly caused by the finite number of available states that can be excited in a material, such as the number of electronic states across the bandgap in a semiconductor. In the realm of single emitters such as single atoms or a single defect in a solid, a single photon can saturate the absorber, switching on and off the system's transmission. The relationship of the absorption coefficient α and the intensity I can often be expressed as:

$$\alpha = \frac{\alpha_0}{1 + \frac{I}{I_S}}$$

where α_0 is the low-intensity absorption coefficient and I_S is the saturation intensity.

SA enables optical modulation of light intensities and can be used as an important building block in photonics and optoelectronics applications. The ultrafast relaxation dynamics of carriers and excitons in 2D materials are favorable for such applications, enabling fast response and tuning, which has been used for passive mode-locking in a cavity for ultrashort laser pulse generation[157–159]. In addition, the operation wavelength window is highly dependent on the material's bandgap,

covering a wide spectral range (Fig. 2a). Graphene-based SAs are notable for their wide wavelength operation range, although it is often desirable to achieve higher modulation depth, which requires strong absorption. Nevertheless, the combination of ultrafast speed and high bandwidth makes these materials promising for high-performance interconnection in optical communication[157].

Another third-order nonlinear absorption process is two-photon absorption (TPA). In TPA, two photons of the same frequency are absorbed simultaneously, promoting an electron from the ground state, such as the valence band, to an excited state, such as the conduction band, with a total energy increase equal to the combined photon energy. TPA occurs only when the energy of a single photon is greater than half the bandgap of the nonlinear material. Unlike saturable absorption, the absorption coefficient in TPA is proportional to the input optical intensity, meaning that the absorption increases with higher intensity.

Two-photon absorption allows for the detection of dark exciton states as it can excite optical species with different selection rules than linear spectroscopy. For instance, excitonic states with nonzero angular momentum, such as 2p and 3p excitons, are usually inaccessible with linear optical detection, can be detected by two-photon excitation spectroscopy[160]. In monolayer WS_2, this enables the measurement of 2p and 3p exciton states[161]. Photoluminescence upconversion has also been reported in monolayer WSe_2[162]. However, when real states such as excitons rather than virtual states are excited, other nonlinear processes such as Auger recombination[163], phonon absorption[164] may start to play a role in addition to two-photon processes[165].

5. High Harmonic Generation

Beyond second and third-order nonlinearity, higher-order nonlinearity can occur under an intense laser field. Specifically, the high harmonic generation (HHG), which occurs under conditions where the optical field is approaching the ionization threshold of materials, has been extensively studied in atomic and molecular gas over the past decades[166], and more recently in solids as well[167]. Different from other lower order nonlinearity, HHG is a nonperturbative process, in the sense that the harmonic yield does not scale as $|E|^q$ as in perturbative nonlinear optics, where q is the order of the harmonics[165]. Instead, a spectral plateau is often observed, over which the efficiency does not significantly vary with harmonic order. In addition, there is often a cut-off frequency, beyond which the harmonic intensity shows a steep drop[168]. The cutoff frequency can be roughly described by a semiclassical model where an electron, after escaping the ion under the influence of the oscillating laser field, recollides with the parent ion, resulting in the emission of high-energy photons[169]. HHG can be used generate ultrafast attosecond pulses, which opens up new avenues for studying various dynamics in solids at the attosecond timescale [8,170–172].

In 2D materials such as a monolayer MoS_2[173], multiple HHG peaks up to 13^{th} order at an integer number of the pump energy is observed. The generated harmonic intensity varies as $\sim I^{3.3}$ for a range of harmonics, demonstrating that HHG is in the non-perturbative regime. Similarly, in artificially stacked R-type multilayer WS_2, the HHG up to the 19^{th} order is observed[174]In this case, both the even- and odd-order harmonic intensity increase quadratically with the number of layers. Similar to other nonlinear processes, phase matching plays an important role in high-harmonic generation and the formation of attosecond laser pulses[175]. The effect of phase matching and potential relaxation thereof in 2D materials remains to be systematically explored.

6. Nonlinear optics in the few-photon regime

While traditional nonlinear optics relies on strong optical fields[176], the emerging field of quantum nonlinear optics seeks to achieve strong nonlinearity with lower power and ultimately even at the few-photon level. This has been a significant goal in both classical and nonclassical optics, as it enables energy-efficient devices such as optical switches, single-photon transistors and gates[177–180]. However, photons, as the fundamental units of light, generally do not interact with each other unless under very specific conditions. One approach to facilitate strong photon-photon interactions is by integrating materials with strong nonlinearities. For example, systems such as single atoms[29,181], molecules[182], and atomic defects in solids[183], where the reflectance and absorption of the particle can be modified by a single photon with inherently strong nonlinearities. Such nonlinearity can be considered as, for instance, third-order nonlinearities such as saturable absorption with a saturation intensity corresponding to one photon per lifetime[184]. However, a major challenge to demonstrate single-photon nonlinearity lies in the deterministic coupling of light to these emitters, such as embedding them in optical resonators[29,180,181,185].

An alternative approach involves using extended optical excitations, such as excitons in semiconductors. Excitons have larger oscillator strengths, which lead to stronger coupling to light, making them a promising candidate for achieving the desired nonlinear interactions[44]. The exciton density dependent resonance leads to third-order nonlinearity, which can be both dispersive and dissipative. The challenge, however, lies in the relatively weak nonlinearities due to the weak interactions among excitons that are charge neutral. For instance, in 2D semiconductors such as monolayer $MoSe_2$ [186], the excitonic nonlinearity induced by the exciton-exciton interaction can be observed as a exciton blueshift under pulsed laser excitation (Fig.7a). The interaction strength, g_{exc}, is defined as the energy shift induced per unit area density of excitons. Rather generally, the exciton-exciton interaction g_{exc}, dominated by exchange interactions is on the order of $\sim E_B R_b^2$, where E_B is the exciton binding energy and R_b is the exciton Bohr radius. Notably, a smaller Bohr radius leads to tighter binding of excitons, which makes g_{exc} more or less agnostic of materials, on the order of $\sim \mu eV \cdot \mu m^2$, whether in TMDs or GaAs quantum wells[187].

One way to enhance exciton nonlinearity is by spatially separating electrons and holes to form interlayer excitons (Fig. 7b). These interlayer excitons experience dipolar interactions, which can be stronger than those of intralayer excitons due to dipolar repulsion. In systems such as bilayer WSe_2[82], bilayer MoS_2[47],WSe_2/hBN/$MoSe_2$[188] and $MoSe_2$/hBN/$MoSe_2$[189], interlayer excitons exhibit a significant energy blueshift in photoluminescence (PL) or absorption as excitation power increases. The interaction strength increases with the electric dipole moment, following the parallel-plate capacitor model to the first order[190], making this nonlinear shift especially pronounced in interlayer excitons with a larger dipole moment, such as those separated by an additional hBN spacer.

It is also reported that the Coulomb interactions between excitons and free carriers can be much stronger than the exciton-exciton interactions and be used to facilitate large optical nonlinearity. For example (Fig.7d,e), in homo-trilayer WSe_2[46], attractive Fermi polaron resonance also shows dramatic nonlinearity under both CW above band laser excitation and pulsed resonance excitations. The nonlinear interaction strength g reaches as large as $\sim 2\ meV \cdot \mu m^2$, significantly larger than exciton-exciton interactions. Interestingly , the nonlinearity only occurs when the

trilayer is doped with holes, but not when it is intrinsic or electron-doped This strong nonlinearity on the hole side was attributed to the valley polarization created by the exciton-carrier scattering, related to the near degenerate K and Γ valleys in such materials[191]. Such enhancement of interactions between optical excitations was also observed for the attractive polaron in $MoSe_2$ whose interaction strength is measured to be more than an order of magnitude stronger than those between bare excitons[192]. Crucially, this experiment characterizes the nonlinearity by exciting the material below its bandgap, which induces virtual populations and AC Stark shift (Fig.7c). This helps to eliminate the complexity of measuring the population and interaction strength of excitons, such as dark excitons. In general, the gate-dependent response provides freedom for electrical tuning of the nonlinearity.

6.1 Engineering nonlinearity through cavity enhancement

Given the intrinsically weak exciton-exciton interactions, various strategies are being pursued to enhance nonlinearity to the few-photon regime. A prominent approach involves integrating optical materials with cavities or waveguides[25,43]. For example, embedding TMDs into optical cavities leads to the formation of exciton-polaritons—a state that is half-light and half-matter—when the energy exchange between photons and excitons occurs faster than their respective decay rates (Fig.8a). This strong light-matter coupling is typically characterized by the emergence of two polariton states with distinct energies, known as the lower and upper polaritons[193]. The coupling strength, also known as vacuum Rabi splitting, can be determined by observing the anti-crossing behavior between excitons and photons (Fig.8b).

Crucially, polaritons often exhibit different nonlinear responses compared to bare excitons. In particular, the nonlinearity of polariton can be expressed as the susceptibility: $\chi^{(3)}(r) = \frac{16 g_{exc-ph}^4}{|\Gamma|^2 \Gamma} \frac{iU(r)}{\Gamma + iU(r)}$, where g_{exc-ph} is the coupling strength between exciton and photon, $U(r)$ as the interaction strength between two excitons with a distance of r and Γ as the linewidth. Meanwhile, the cavity modifies the linewidth of the excitons, often reducing the number of photons required to shift the resonance by a linewidth. Last but not least, with increasing pumping intensity, the vacuum Rabi splitting between the two polaritons also decreases, leading to the energy shift of polaritons[194,195]. The reduction in the splitting is due to the phase-space filling[48], where more exciton population leads to fewer excitons left to couple to the cavity photon, similar to saturable absorption. In fact, the Rabi splitting strength Ω depends on the polariton density: $\Omega = 2g\left(1 - \frac{n\pi R_b^2}{2}\right), leading\ to$ phase-space filling induced nonlinearity $g_{pol-pol} \propto a_b^2 \hbar \Omega$[196].

TMDs offer several appealing features for exploring the nonlinear interaction of polaritons in the strong light-matter coupling regime. With excitons in TMDs possessing large binding energies ranging from 200 to 500 meV and large oscillator strengths, strong coupling can persist even at room temperature with possibly enhanced exciton-mediated nonlinearity[197]. The nonlinearity of polaritons generated in TMDs varies significantly depending on the specific species coupled to the cavity photon. For instance (Fig.8f), in monolayer WSe_2, the 2s exciton-polaritons exhibit a larger nonlinearity of approximately $46.4 \pm 13.9\ \mu eV \cdot \mu m^2$, which is about four times larger than that of the 1s state[48]. This difference is expected, given the larger Bohr radius of 2s exciton. Leveraging this, biexciton polariton also exhibits nonlinear interaction boost[198]. Phase space filling was thought to play an important role in the measured nonlinear response in TMD polaritons. Similarly, trion-polariton in monolayer $MoSe_2$ microcavity exhibits enhancement on the

nonlinearity strength of ~$37 \pm 3\ \mu eV \cdot \mu m^2$ at a low electron density and pump fluence[199] driven by the strong band-filling effect. However, the increased nonlinearity observed in 2s exciton- and trion-polaritons comes at the cost of reduced coupling strength between the optical excitation and the photons due to their weaker oscillator strength.

Another approach uses interlayer excitons with stronger dipolar repulsion, such as those in bilayer MoS_2, interlayer excitons[47](Fig.8c). Such interlayer excitons in fact can have sufficient oscillator strength to enable strong coupling when the carrier tunneling is the materials is large enough to produce enough hybridization between interlayer and intralayer[112]. Combining this IX exciton with cavity photons forms the dipolar interlayer polariton, which has a ten-fold enhancement of this nonlinearity strength (g_{IX}~ $100\pm2\ \mu eV\ \mu m^2$) compared with the conventional intralayer exciton (A) (g_A~ $10\pm0.2\ \mu eV\ \mu m^2$)) embedded in microcavity[47,200].

Similar to excitons in a cavity, it has been proposed[201] that one can significantly reduce the linewidth of the excitons by placing the monolayer $MoSe_2$ close to a partially reflecting mirror with a half-integer multiple of the exciton resonance wavelength. This could be understood as the destructive interference between the reflected light from the mirror and the emitted light from TMD substantially suppressing the radiative linewidth, leading to the formation of long-lived polariton, a hybrid of photon and exciton. Such reduction in linewidth reduces the number of photons required for shifting the exciton energy by a linewidth.

An intriguing set of recent experiments uses the moiré superlattice in 2D materials to demonstrate strong nonlinearity in exciton-polariton systems[202](Fig.8d,e). With the moiré excitons are confined within each site, they experience strong on-site interaction[203–205], which suggests that the exciton blockade can occur when average exciton-exciton density is close to the size of the moiré cell, on the order of a few to tens of nanometers, much larger than the blockade radius of bare excitons. Meanwhile, the exciton and photon can still couple collectively among all the cells, which maintains the system in a strong coupling regime.

With their recent development, it has become more feasible for this system to finally enter the quantum nonlinear optics regime when the polariton nonlinear interaction strength surpasses the linewidth. In such cases, the optical response of the system is significantly altered by the presence of a single photon, leading to unprecedented phenomena and technologies in solids. One of such examples is the so-called photon blockade[206,207], where a single polariton can inhibit the transmission of additional photons. Such photon blockade effect can be observed through photon antibunching and could open exciting avenues for realizing nonclassical light sources in quantum nonlinear optics[102,208–210].

7. Outlook

We have reviewed the various opportunities that 2D materials present in nonlinear optics, spanning both classical and quantum regimes. Critically, 2D materials offer significant advantages by enabling the fabrication of novel heterostructures with well-controlled symmetry and band structures, leading to nonlinear optical responses often unattainable in bulk crystals. Moreover, the properties of these materials can be highly tunable under different perturbations, unlocking new functionalities for tuning and transducing nonlinear optical signals. Their atomically thin nature also introduces novel mechanisms for nonlinear processes, such as relaxing phase-matching

conditions. The potential to integrate these heterostructures into various technological platforms, such as photonic integrated circuits, is particularly appealing for the development of nonlinear optical circuits[211–214].

Despite their highly desirable features and significant recent progress, key challenges remain in developing nonlinear optical technologies using 2D materials. Many fundamental questions still exist regarding the basic understanding of optical nonlinearity in these materials. The physical mechanisms of interactions, radiative vs. non-radiative decay, dephasing of optical excitations, and the roles of dark states—crucial parameters for optical nonlinearity—are not well understood for many 2D materials[215]. For example, how can one determine the population of dark excitons versus bright excitons to measure their interaction strength accurately? Additionally, while lattice relaxation at the interface of 2D heterostructures is well known, its influence on lattice dynamics and optical nonlinearity remains unclear[216]. Addressing these questions requires both the development of new theoretical models and novel instrumentation and methods capable of probing such phenomena at ultrafast timescales or ultrasmall length scales below the diffraction limit, which would, in turn, open a new frontier in the nonlinear optical science.

Beyond these challenges in our fundamental understanding of optical nonlinearity, there are technical obstacles to building efficient nonlinear optical devices with 2D materials. While their atomically thin nature gives rise to unique nonlinear properties, it also significantly limits the overall efficiency of processes like frequency conversion due to the much shorter interaction distance[217]. Reassembling these monolayers into thicker layers could help address this limitation, but precise control over the material's symmetry and band structure is required to maintain a strong nonlinear response. Furthermore, as the thickness increases, phase-matching conditions become critical once again[93]. A potential solution involves fabricating multi-layer structures where active nonlinear materials are sandwiched between passive linear materials to compensate for phase mismatch. To create viable technologies, however, these complex structures must be scalable, potentially through direct growth methods.

For quantum nonlinear optics applications, enhancing the interaction strength among optical excitations and reducing their linewidth is particularly desirable. Spatial confinement of excitons can significantly lower the number of photons required to achieve blockade, which may be achieve via moiré superlattice[202,218–220], strain engineering[86,221], and electrostatic gating[222]. Additionally, engineering the resonance linewidth through cavity quantum electrodynamics, as well as improving material quality, can further reduce such photon threshold. The short radiative lifetime of excitons, stemming from their intrinsically large oscillator strength[223], is advantageous for creating single-photon sources with high repetition rates and optical switches with ultrafast operation. However, these fast dynamics pose challenges in measuring photon statistics and exciton behavior, which calls for the development of innovative optical measurement techniques[224,225].

From the materials perspective, the application of 2D materials in optical devices requires the growth of wafer-scale high quality 2D materials, which remains challenging due to difficulties in controlling crystallinity, defects, and stoichiometry in these atomically thin films[226,227]. The direct growth of phase-pure films on non-lattice-matched substrates, such as silicon and oxides, in a CMOS-compatible process is an area that demands significant effort[228]. In the realm of creating moiré or twisted heterostructures, while current methods of stacking 2D materials into heterostructures offers remarkable flexibility by relaxing lattice-matching requirements and

introducing the twist degree of freedom, they also often result in large variations in interfacial structure, leading to device variability[229,230]. Ultimately, more scalable methods to fabricate van der Waals heterostructures with nanometric precision, either via transfer or growth, are needed for optical technologies[231]. Realizing novel nonlinear optical technologies based on 2D materials will thus require multidisciplinary collaborative efforts between physicists, materials scientists, optical engineers, and device designers.

Acknowledgements:

This research is supported by the U.S. Department of Energy, Office of Science, Office of Basic Energy Sciences Early Career Research Program under Award No. DE-SC-0022885 and the National Science Foundation CAREER Award under Award No. DMR-2145712.

Reference:

1. Boyd, R. W. *Nonlinear Optics*. (Elsevier, 2020).
2. Shen, Y. R. *Principles Of Nonlinear Optics*. (John Wiley and Sons (WIE), New York, NY, 1984).
3. Bloembergen, N. Nonlinear optics and spectroscopy. *Science* **216**, 1057–1064 (1982).
4. Keszler, D. A. Borates for optical frequency conversion. *Curr. Opin. Solid State Mater. Sci.* **1**, 204–211 (1996).
5. Eisert, J., Friesdorf, M. & Gogolin, C. Quantum many-body systems out of equilibrium. *Nat. Phys.* **11**, 124–130 (2015).
6. Hartmann, M. J. Quantum simulation with interacting photons. *J. Opt.* **18**, 104005 (2016).
7. Noh, C. & Angelakis, D. G. Quantum simulations and many-body physics with light. *Rep. Prog. Phys.* **80**, 016401 (2017).
8. Krausz, F. & Ivanov, M. Attosecond physics. *Rev. Mod. Phys.* **81**, 163–234 (2009).
9. Keller, U. Recent developments in compact ultrafast lasers. *Nature* **424**, 831–838 (2003).
10. Peccianti, M. *et al.* Demonstration of a stable ultrafast laser based on a nonlinear microcavity. *Nat. Commun.* **3**, 765 (2012).
11. Dudley, J. M., Genty, G. & Coen, S. Supercontinuum generation in photonic crystal fiber. *Rev. Mod. Phys.* **78**, 1135–1184 (2006).
12. Alfano, R. R. & Shapiro, S. L. Observation of self-phase modulation and small-scale filaments in crystals and glasses. *Phys. Rev. Lett.* **24**, 592–594 (1970).
13. Wright, L. G., Christodoulides, D. N. & Wise, F. W. Controllable spatiotemporal nonlinear effects in multimode fibres. *Nat. Photonics* **9**, 306–310 (2015).
14. Sun, Z., Martinez, A. & Wang, F. Optical modulators with 2D layered materials. *Nat. Photonics* **10**, 227–238 (2016).
15. Reed, G. T., Mashanovich, G., Gardes, F. Y. & Thomson, D. J. Silicon optical modulators. *Nat. Photonics* **4**, 518–526 (2010).
16. Klein, M. *et al.* 2D semiconductor nonlinear plasmonic modulators. *Nat. Commun.* **10**, 3264 (2019).
17. Agrawal, G. P. Nonlinear fiber optics: its history and recent progress [Invited]. *J. Opt. Soc. Am. B, JOSAB* **28**, A1–A10 (2011).

18. Feng, X. *et al.* Dispersion controlled highly nonlinear fibers for all-optical processing at telecoms wavelengths. *Opt. Fiber Technol.* **16**, 378–391 (2010).
19. Saitoh, K. & Koshiba, M. Highly nonlinear dispersion-flattened photonic crystal fibers for supercontinuum generation in a telecommunication window. *Opt. Express* **12**, 2027–2032 (2004).
20. Gu, T. *et al.* Regenerative oscillation and four-wave mixing in graphene optoelectronics. *Nat. Photonics* **6**, 554–559 (2012).
21. Chergui, M., Beye, M., Mukamel, S., Svetina, C. & Masciovecchio, C. Progress and prospects in nonlinear extreme-ultraviolet and X-ray optics and spectroscopy. *Nat Rev Phys* **5**, 578–596 (2023).
22. Dudovich, N., Oron, D. & Silberberg, Y. Single-pulse coherently controlled nonlinear Raman spectroscopy and microscopy. *Nature* **418**, 512–514 (2002).
23. Helmchen, F. & Denk, W. Deep tissue two-photon microscopy. *Nat. Methods* **2**, 932–940 (2005).
24. Parodi, V. *et al.* Nonlinear Optical Microscopy: From Fundamentals to Applications in Live Bioimaging. *Front. Bioeng. Biotechnol.* **8**, (2020).
25. Chang, D. E., Vuletić, V. & Lukin, M. D. Quantum nonlinear optics — photon by photon. *Nat. Photonics* **8**, 685–694 (2014).
26. Sultanov, V. *et al.* Tunable entangled photon-pair generation in a liquid crystal. *Nature* **631**, 294–299 (2024).
27. Dorfman, K. E., Schlawin, F. & Mukamel, S. Nonlinear optical signals and spectroscopy with quantum light. *Rev. Mod. Phys.* **88**, 045008 (2016).
28. Caspani, L. *et al.* Integrated sources of photon quantum states based on nonlinear optics. *Light Sci. Appl.* **6**, e17100 (2017).
29. Birnbaum, K. M. *et al.* Photon blockade in an optical cavity with one trapped atom. *Nature* **436**, 87–90 (2005).
30. Wang, J., Sciarrino, F., Laing, A. & Thompson, M. Integrated photonic quantum technologies. *Nat. Photonics* **14**, 273–284 (2019).
31. Miller, D. A. B. Are optical transistors the logical next step? *Nat. Photonics* **4**, 3–5 (2010).
32. Kimble, H. J. The Quantum Internet. *Nature* **453**, 1023–1030 (2008).
33. Wang, Y., Jöns, K. & Sun, Z. Integrated photon-pair sources with nonlinear optics. *Appl. Phys. Rev.* **8**, 011314 (2021).
34. Ferrera, M. *et al.* Low-power continuous-wave nonlinear optics in doped silica glass integrated waveguide structures. *Nature photonics* **2**, 737–740 (2008).
35. Zhang, M., Wang, C., Kharel, P., Zhu, D. & Lončar, M. Integrated lithium niobate electro-optic modulators: when performance meets scalability. *Optica* **8**, 652 (2021).
36. Wang, C. *et al.* Integrated lithium niobate electro-optic modulators operating at CMOS-compatible voltages. *Nature* **562**, 101–104 (2018).
37. Sasaki, T., Mori, Y., Yoshimura, M., Yap, Y. K. & Kamimura, T. Recent development of nonlinear optical borate crystals: key materials for generation of visible and UV light. *Mater. Sci. Eng. R Rep.* **30**, 1–54 (2000).
38. Wang, Q. H., Kalantar-Zadeh, K., Kis, A., Coleman, J. N. & Strano, M. S. Electronics and optoelectronics of two-dimensional transition metal dichalcogenides. *Nat. Nanotechnol.* **7**, 699–712 (2012).
39. Geim, A. K. Graphene: status and prospects. *Science* **324**, 1530–1534 (2009).

40. Xu, Y., Shi, Z., Shi, X., Zhang, K. & Zhang, H. Recent progress in black phosphorus and black-phosphorus-analogue materials: properties, synthesis and applications. *Nanoscale* **11**, 14491–14527 (2019).
41. Novoselov, K. S., Mishchenko, A., Carvalho, A. & Castro Neto, A. H. 2D materials and van der Waals heterostructures. *Science* **353**, aac9439 (2016).
42. Liu, X. & Hersam, M. C. 2D materials for quantum information science. *Nat. Rev. Mater.* **4**, 669–684 (2019).
43. Luo, Y. *et al.* Strong light-matter coupling in van der Waals materials. *Light Sci. Appl.* **13**, 203 (2024).
44. Wang, G. *et al.* Colloquium : Excitons in atomically thin transition metal dichalcogenides. *Rev. Mod. Phys.* **90**, 021001 (2018).
45. Wilson, N. P., Yao, W., Shan, J. & Xu, X. Excitons and emergent quantum phenomena in stacked 2D semiconductors. *Nature* **599**, 383–392 (2021).
46. Gu, L. *et al.* Giant optical nonlinearity of Fermi polarons in atomically thin semiconductors. *Nat. Photonics* **18**, 816–822 (2024).
47. Datta, B. *et al.* Highly nonlinear dipolar exciton-polaritons in bilayer MoS_2. *Nat. Commun.* **13**, 6341 (2022).
48. Gu, J. *et al.* Enhanced nonlinear interaction of polaritons via excitonic Rydberg states in monolayer WSe_2. *Nat. Commun.* **12**, 2269 (2021).
49. Wang, H.-X. *et al.* Quantum many-body simulation using monolayer exciton-polaritons in coupled-cavities. *J. Phys. Condens. Matter* **29**, 445703 (2017).
50. Englund, D. *et al.* Ultrafast photon-photon interaction in a strongly coupled quantum dot-cavity system. *Phys. Rev. Lett.* **108**, 093604 (2012).
51. Geim, A. K. & Grigorieva, I. V. Van der Waals heterostructures. *Nature* **499**, 419–425 (2013).
52. Li, P. *et al.* Infrared hyperbolic metasurface based on nanostructured van der Waals materials. *Science* **359**, 892–896 (2018).
53. Errando-Herranz, C. *et al.* Resonance fluorescence from waveguide-coupled, strain-localized, two-dimensional quantum emitters. *ACS Photonics* **8**, 1069–1076 (2021).
54. Zhang, Q. *et al.* Interface nano-optics with van der Waals polaritons. *Nature* **597**, 187–195 (2021).
55. Fejer, M. M., Magel, G. A., Jundt, D. H. & Byer, R. L. Quasi-phase-matched second harmonic generation: tuning and tolerances. *IEEE J. Quantum Electron.* **28**, 2631–2654 (1992).
56. Mak, K. & Shan, J. Photonics and optoelectronics of 2D semiconductor transition metal dichalcogenides. *Nat. Photonics* **10**, 216–226 (2016).
57. Akinwande, D. *et al.* Graphene and two-dimensional materials for silicon technology. *Nature* **573**, 507–518 (2019).
58. Young, A. F. & Kim, P. Electronic transport in graphene heterostructures. *Annu. Rev. Condens. Matter Phys.* **2**, 101–120 (2011).
59. Dogadov, O., Trovatello, C., Yao, B., Soavi, G. & Cerullo, G. Parametric nonlinear optics with layered materials and related heterostructures. *Laser Photon. Rev.* **16**, 2100726 (2022).
60. Autere, A. *et al.* Nonlinear optics with 2D layered materials. *Adv. Mater.* **30**, e1705963 (2018).
61. Xie, Z., Zhao, T., Yu, X. & Wang, J. Nonlinear Optical Properties of 2D Materials and their Applications. *Small* **20**, e2311621 (2024).
62. Wang, Y., Xiao, J., Yang, S., Wang, Y. & Zhang, X. Second harmonic generation spectroscopy on two-dimensional materials [Invited]. *Opt. Mater. Express* **9**, 1136 (2019).

63. Manzeli, S., Ovchinnikov, D., Pasquier, D., Yazyev, O. V. & Kis, A. 2D transition metal dichalcogenides. *Nat. Rev. Mater.* **2**, 17033 (2017).
64. Splendiani, A. *et al.* Emerging photoluminescence in monolayer MoS_2. *Nano Lett.* **10**, 1271–1275 (2010).
65. Mak, K. F., Lee, C., Hone, J., Shan, J. & Heinz, T. F. Atomically thin MoS_2: a new direct-gap semiconductor. *Phys. Rev. Lett.* **105**, 136805 (2010).
66. Zhao, M. *et al.* Atomically phase-matched second-harmonic generation in a 2D crystal. *Light Sci. Appl.* **5**, e16131 (2016).
67. Shi, J. *et al.* 3R MoS2 with broken inversion symmetry: A promising ultrathin nonlinear optical device. *Adv. Mater.* **29**, (2017).
68. Withers, F. *et al.* Light-emitting diodes by band-structure engineering in van der Waals heterostructures. *Nat. Mater.* **14**, 301–306 (2015).
69. Ni, G. X. *et al.* Plasmons in graphene moiré superlattices. *Nat. Mater.* **14**, 1217–1222 (2015).
70. Fei, Z. *et al.* Gate-tuning of graphene plasmons revealed by infrared nano-imaging. *Nature* **487**, 82–85 (2012).
71. Caldwell, J. D. *et al.* Low-loss, infrared and terahertz nanophotonics using surface phonon polaritons. *Nanophotonics* **4**, 44–68 (2015).
72. Dai, S. *et al.* Tunable phonon polaritons in atomically thin van der Waals crystals of boron nitride. *Science* **343**, 1125–1129 (2014).
73. Dufferwiel, S. *et al.* Exciton-polaritons in van der Waals heterostructures embedded in tunable microcavities. *Nat. Commun.* **6**, 8579 (2015).
74. Gan, X. *et al.* Controlling the spontaneous emission rate of monolayer MoS_2 in a photonic crystal nanocavity. *Appl. Phys. Lett.* **103**, 181119 (2013).
75. Liu, X. *et al.* Strong light–matter coupling in two-dimensional atomic crystals. *Nat. Photonics* **9**, 30–34 (2015).
76. Gullans, M., Chang, D. E., Koppens, F. H. L., García de Abajo, F. J. & Lukin, M. D. Single-photon nonlinear optics with graphene plasmons. *Phys. Rev. Lett.* **111**, 247401 (2013).
77. Yin, X. *et al.* Edge nonlinear optics on a MoS_2 atomic monolayer. *Science* **344**, 488–490 (2014).
78. Chernikov, A. *et al.* Exciton binding energy and nonhydrogenic Rydberg series in monolayer WS_2. *Phys. Rev. Lett.* **113**, 076802 (2014).
79. Li, Y. *et al.* Measurement of the optical dielectric function of monolayer transition-metal dichalcogenides:MoS2,MoSe2,WS2, andWSe2. *Phys rev B* **90**, 205422 (2014).
80. Wang, G. *et al.* Giant enhancement of the optical second-harmonic emission of WSe_2 monolayers by laser excitation at exciton resonances. *Phys. Rev. Lett.* **114**, 097403 (2015).
81. Soh, D. B. S., Rogers, C., Gray, D. J., Chatterjee, E. & Mabuchi, H. Optical nonlinearities of excitons in monolayer MoS_2. *Phys. Rev. B.* **97**, 1–21 (2018).
82. Wang, Z., Chiu, Y.-H., Honz, K., Mak, K. F. & Shan, J. Electrical tuning of interlayer exciton gases in WSe_2 bilayers. *Nano Lett.* **18**, 137–143 (2018).
83. Hagel, J., Brem, S. & Malic, E. Electrical tuning of moiré excitons in $MoSe_2$ bilayers. *2d Mater.* **10**, 014013 (2023).
84. Aslan, B., Deng, M. & Heinz, T. F. Strain tuning of excitons in monolayer WSe_2. *Phys. Rev. B.* **98**, 115308 (2018).
85. Bai, Y. *et al.* Excitons in strain-induced one-dimensional moiré potentials at transition metal dichalcogenide heterojunctions. *Nat. Mater.* **19**, 1068–1073 (2020).

86. Guan, Z. *et al.* Giant second-order susceptibility in monolayer WSe_2 via strain engineering. *arXiv*.2407.21296 (2024).
87. Glazov, M. M., Golub, L. E., Wang, G., Marie, X. & Amand, T. Intrinsic exciton-state mixing and nonlinear optical properties in transition metal dichalcogenide monolayers. *Phys. Rev. B.* **95**, 035311 (2017).
88. Mak, K. F., He, K., Shan, J. & Heinz, T. F. Control of valley polarization in monolayer MoS_2 by optical helicity. *Nat. Nanotechnol.* **7**, 494–498 (2012).
89. Zeng, H., Dai, J., Yao, W., Xiao, D. & Cui, X. Valley polarization in MoS_2 monolayers by optical pumping. *Nat. Nanotechnol.* **7**, 490–493 (2012).
90. Sallen, G. *et al.* Robust optical emission polarization in MoS_2 monolayers through selective valley excitation. *Phys. Rev. B.* **86**, 081301 (2012).
91. Alireza Taghizadeh, T. G. P. Nonlinear optical selection rules of excitons in monolayer transition metal dichalcogenides. *Physics Review B* **99**, 1–11 (2019).
92. Zhang, Y. *et al.* Coherent modulation of chiral nonlinear optics with crystal symmetry. *Light Sci. Appl.* **11**, 216 (2022).
93. Xu, X. *et al.* Towards compact phase-matched and waveguided nonlinear optics in atomically layered semiconductors. *Nat. Photonics* **16**, 698–706 (2022).
94. Ciattoni, A., Marini, A., Rizza, C. & Conti, C. Phase-matching-free parametric oscillators based on two-dimensional semiconductors. *Light Sci. Appl.* **7**, 5 (2018).
95. You, J. W., Bongu, S. R., Bao, Q. & Panoiu, N. C. Nonlinear optical properties and applications of 2D materials: theoretical and experimental aspects. *Nanophotonics* **8**, 63–97 (2018).
96. Muhammad, N., Chen, Y., Qiu, C.-W. & Wang, G. P. Optical bound states in continuum in MoS2-based metasurface for directional light emission. *Nano Lett.* **21**, 967–972 (2021).
97. Thureja, D. *et al.* Electrically tunable quantum confinement of neutral excitons. *Nature* **606**, 298–304 (2022).
98. Jin, C. *et al.* Ultrafast dynamics in van der Waals heterostructures. *Nat. Nanotechnol.* **13**, 994–1003 (2018).
99. Yu, S., Wu, X., Wang, Y., Guo, X. & Tong, L. 2D materials for optical modulation: Challenges and opportunities. *Adv. Mater.* **29**, 1606128 (2017).
100. Youngblood, N. & Li, M. Integration of 2D materials on a silicon photonics platform for optoelectronics applications. *Nanophotonics* **6**, 1205–1218 (2016).
101. Montblanch, A. R.-P., Barbone, M., Aharonovich, I., Atatüre, M. & Ferrari, A. C. Layered materials as a platform for quantum technologies. *Nat. Nanotechnol.* **18**, 555–571 (2023).
102. Turunen, M. *et al.* Quantum photonics with layered 2D materials. *Nat. Rev. Phys.* **4**, 219–236 (2022).
103. Shen, Y. R. Surface properties probed by second-harmonic and sum-frequency generation. *Nature* **337**, 519–525 (1989).
104. Fan, X. *et al.* Broken Symmetry Induced Strong Nonlinear Optical Effects in Spiral WS_2 Nanosheets. *ACS Nano* **11**, 4892–4898 (2017).
105. Malard, L. M., Alencar, T. V., Barboza, A. P. M., Mak, K. F. & de Paula, A. M. Observation of intense second harmonic generation from MoS2atomic crystals. *Phys. Rev. B.* **87**, 201401 (2013).
106. Liu, F. *et al.* Disassembling 2D van der Waals crystals into macroscopic monolayers and reassembling into artificial lattices. *Science* **367**, 903–906 (2020).

107. Qin, B. *et al.* Interfacial epitaxy of multilayer rhombohedral transition-metal dichalcogenide single crystals. *Science* **385**, 99–104 (2024).
108. Lafrentz, M. *et al.* Second-harmonic generation spectroscopy of excitons in ZnO. *Phys. Rev. B* **88**, 235207 (2013).
109. Wang, K. *et al.* Electrical control of charged carriers and excitons in atomically thin materials. *Nat. Nanotechnol.* **13**, 128–132 (2018).
110. Seyler, K. L. *et al.* Electrical control of second-harmonic generation in a WSe_2 monolayer transistor. *Nat. Nanotechnol.* **10**, 407–411 (2015).
111. Shree, S. *et al.* Interlayer exciton mediated second harmonic generation in bilayer MoS_2. *Nat. Commun.* **12**, 6894 (2021).
112. Leisgang, N. *et al.* Giant Stark splitting of an exciton in bilayer MoS_2. *Nat. Nanotechnol.* **15**, 901–907 (2020).
113. Klein, J. *et al.* Electric-field switchable second-harmonic generation in bilayer MoS_2 by inversion symmetry breaking. *Nano Lett.* **17**, 392–398 (2017).
114. Cha, S. *et al.* Enhancing resonant second harmonic generation in bilayer WSe_2 by layer-dependent exciton-polaron effect. *arXiv.*2407.01854 (2024).
115. Nikogosyan, D. N. *Nonlinear Optical Crystals: A Complete Survey*. (Springer, New York, NY, 2005).
116. Zhou, R., Krasnok, A., Hussain, N., Yang, S. & Ullah, K. Controlling the harmonic generation in transition metal dichalcogenides and their heterostructures. *Nanophotonics* **11**, 3007–3034 (2022).
117. Rhim, S. H., Kim, Y. S. & Freeman, A. J. Strain-induced giant second-harmonic generation in monolayered 2H-MoX_2 (X= S, Se, Te). *Appl. Phys. Lett.* (2015).
118. Beach, K., Lucking, M. C. & Terrones, H. Strain dependence of second harmonic generation in transition metal dichalcogenide monolayers and the fine structure of the C exciton. *Phys. Rev. B.* **101**, (2020).
119. Tan, S. J. R. *et al.* Chemical Stabilization of 1T′ Phase Transition Metal Dichalcogenides with Giant Optical Kerr Nonlinearity. *J. Am. Chem. Soc.* **139**, 2504–2511 (2017).
120. Kumar, N. *et al.* Second harmonic microscopy of monolayer MoS_2. *Phys. Rev. B* **87**, 161403 (2013).
121. Zhao, Y., Chen, Z., Wang, C., Yang, Y. & Sun, H. B. Efficient second-and higher-order harmonic generation from LiNbO 3 metasurfaces. *Nanoscale* **15**, 12926–12932 (2023).
122. Martorell, J., Vilaseca, R. & Corbalán, R. Second harmonic generation in a photonic crystal. *Appl. Phys. Lett.* **70**, 702–704 (1997).
123. Bloembergen, N., Chang, R. K., Jha, S. S. & Lee, C. H. Optical second-harmonic generation in reflection from media with inversion symmetry. *Phys. Rev.* **174**, 813–822 (1968).
124. Yariv, A. & Louisell, W. Theory of the optical parametric oscillator. *IEEE Journal of Quantum Electronics* **2**, 118–118 (1966).
125. Giordmaine, J. A. & Miller, R. C. Tunable coherent parametric oscillation in $LiNbO_3$ at optical frequencies. *Phys. Rev. Lett.* **14**, 973–976 (1965).
126. Giordmaine, J. A. Mixing of light beams in crystals. *Phys. Rev. Lett.* **8**, 19–20 (1962).
127. Canalias, C. & Pasiskevicius, V. Mirrorless optical parametric oscillator. *Nat. Photonics* **1**, 459–462 (2007).
128. Trovatello, C. *et al.* Optical parametric amplification by monolayer transition metal dichalcogenides. *Nat. Photonics* **15**, 6–10 (2021).

129. Yang, J. *et al.* Titanium:sapphire-on-insulator integrated lasers and amplifiers. *Nature* **630**, 853–859 (2024).
130. Zhang, Z. *et al.* Large-Scale Spectral Broadening of Femtosecond Optical Parametric Oscillators by $MoTe_2$ Films. *ACS Photonics* **11**, 1044–1050 (2024).
131. Wang, G. *et al.* Tunable nonlinear refractive index of two-dimensional MoS_2, WS_2, and $MoSe_2$ nanosheet dispersions [Invited]. *Photonics Res.* **3**, A51 (2015).
132. Catalano, J. Spontaneous parametric down-conversion and quantum entanglement. (Portland State University Library, 2017). doi:10.15760/honors.474.
133. Kwiat, P. G., Waks, E., White, A. G., Appelbaum, I. & Eberhard, P. H. Ultrabright source of polarization-entangled photons. *Phys. Rev. A* **60**, R773–R776 (1999).
134. Orieux, A., Versteegh, M. A. M., Jöns, K. D. & Ducci, S. Semiconductor devices for entangled photon pair generation: a review. *Rep. Prog. Phys.* **80**, 076001 (2017).
135. Li, X., Voss, P. L., Sharping, J. E. & Kumar, P. Optical-fiber source of polarization-entangled photons in the 1550 nm telecom band. *Phys. Rev. Lett.* **94**, 053601 (2005).
136. Guo, Q. *et al.* Ultrathin quantum light source with van der Waals $NbOCl_2$ crystal. *Nature* **613**, 53–59 (2023).
137. Weissflog, M. A. *et al.* A tunable transition metal dichalcogenide entangled photon-pair source. *Nat. Commun.* **15**, 7600 (2024).
138. Feng, J. *et al.* Polarization-entangled photon-pair source with van der Waals 3R-WS_2 crystal. *eLight* **4**, 16 (2024).
139. Okoth, C., Cavanna, A., Santiago-Cruz, T. & Chekhova, M. V. Microscale generation of entangled photons without momentum conservation. *Phys. Rev. Lett.* **123**, 263602 (2019).
140. Li, L. *et al.* Metalens-array-based high-dimensional and multiphoton quantum source. *Science* **368**, 1487–1490 (2020).
141. Santiago-Cruz, T. *et al.* Resonant metasurfaces for generating complex quantum states. *Science* **377**, 991–995 (2022).
142. Hamel, D. R. *et al.* Direct generation of three-photon polarization entanglement. *Nat. Photonics* **8**, 801–807 (2014).
143. Zhang, Z. *et al.* High-performance quantum entanglement generation via cascaded second-order nonlinear processes. *Npj Quantum Inf.* **7**, 1–9 (2021).
144. Javid, U. A. *et al.* Ultrabroadband entangled photons on a nanophotonic chip. *Phys. Rev. Lett.* **127**, 183601 (2021).
145. Moss, D. Third-order nonlinear optical response of 2D materials in the telecom band. *arXiv.*2403.03441 (2023)
146. Bristow, A. D., Rotenberg, N. & Van Driel, H. M. Two-photon absorption and Kerr coefficients of silicon for 850--2200nm. *Appl. Phys. Lett.* **90**, (2007).
147. Ikeda, K., Saperstein, R. E., Alic, N. & Fainman, Y. Thermal and Kerr nonlinear properties of plasma-deposited silicon nitride/ silicon dioxide waveguides. *Opt. Express* **16**, 12987 (2008).
148. Tsang, T. Y. Optical third-harmonic generation at interfaces. *Phys. Rev. A* **52**, 4116–4125 (1995).
149. Siemens, M. E., Moody, G., Li, H., Bristow, A. D. & Cundiff, S. T. Resonance lineshapes in two-dimensional Fourier transform spectroscopy. *Opt. Express* **18**, 17699–17708 (2010).
150. Bristow, A. D. *et al.* A versatile ultrastable platform for optical multidimensional Fourier-transform spectroscopy. *Rev. Sci. Instrum.* **80**, 073108 (2009).

151. Cundiff, S. T. *et al.* Optical 2-D Fourier transform spectroscopy of excitons in semiconductor nanostructures. *IEEE J. Sel. Top. Quantum Electron.* **18**, 318–328 (2012).
152. Moody, G. *et al.* Intrinsic homogeneous linewidth and broadening mechanisms of excitons in monolayer transition metal dichalcogenides. *Nat. Commun.* **6**, 8315 (2015).
153. Jakubczyk, T. *et al.* Radiatively limited dephasing and exciton dynamics in $MoSe_2$ monolayers revealed with four-wave mixing microscopy. *Nano Lett.* **16**, 5333–5339 (2016).
154. Helmrich, S. *et al.* Phonon-assisted intervalley scattering determines ultrafast exciton dynamics in $MoSe_2$ bilayers. *Phys. Rev. Lett.* **127**, 157403 (2021).
155. Huang, D. *et al.* Quantum dynamics of attractive and repulsive polarons in a doped $MoSe_2$ monolayer. *Phys. Rev. X.* **13**, 011029 (2023).
156. Hao, K. *et al.* Direct measurement of exciton valley coherence in monolayer WSe_2. *Nat. Phys.* **12**, 677–682 (2016).
157. Ma, C. *et al.* Recent progress in ultrafast lasers based on 2D materials as a saturable absorber. *Appl. Phys. Rev.* **6**, 041304 (2019).
158. Liu, W. *et al.* Recent Advances of 2D Materials in Nonlinear Photonics and Fiber Lasers. *Advanced Optical Materials* **8**, (2020).
159. Sun, Z. *et al.* Graphene mode-locked ultrafast laser. *ACS Nano* **4**, 803–810 (2010).
160. Wang, F., Dukovic, G., Brus, L. E. & Heinz, T. F. The optical resonances in carbon nanotubes arise from excitons. *Science* **308**, 838–841 (2005).
161. Ye, Z. *et al.* Probing excitonic dark states in single-layer tungsten disulphide. *Nature* **513**, 214–218 (2014).
162. Manca, M. *et al.* Enabling valley selective exciton scattering in monolayer WSe_2 through upconversion. *Nat. Commun.* **8**, 14927 (2017).
163. Han, B. *et al.* Exciton states in monolayer $MoSe_2$ and $MoTe_2$ probed by upconversion spectroscopy. *Phys. Rev. X.* **8**, (2018).
164. Wang, Q. *et al.* High-energy gain upconversion in monolayer tungsten disulfide photodetectors. *Nano Lett.* **19**, 5595–5603 (2019).
165. Yu, Y. *et al.* Fundamental limits of exciton-exciton annihilation for light emission in transition metal dichalcogenide monolayers. *Phys. Rev. B.* **93**, (2016).
166. Ferray, M. *et al.* Multiple-harmonic conversion of 1064 nm radiation in rare gases. *J. Phys. B At. Mol. Opt. Phys.* **21**, L31–L35 (1988).
167. Ghimire, S. *et al.* Observation of high-order harmonic generation in a bulk crystal. *Nat. Phys.* **7**, 138–141 (2011).
168. Krause, J. L., Schafer, K. J. & Kulander, K. C. High-order harmonic generation from atoms and ions in the high intensity regime. *Phys. Rev. Lett.* **68**, 3535–3538 (1992).
169. Corkum, P. B. Plasma perspective on strong field multiphoton ionization. *Phys. Rev. Lett.* **71**, 1994–1997 (1993).
170. Corkum, P. B. & Krausz, F. Attosecond science. *Nat. Phys.* **3**, 381–387 (2007).
171. Vampa, G. *et al.* All-optical reconstruction of crystal band structure. *Phys. Rev. Lett.* **115**, 193603 (2015).
172. Goulielmakis, E. & Brabec, T. High harmonic generation in condensed matter. *Nat. Photonics* **16**, 411–421 (2022).
173. Liu, H. *et al.* High-harmonic generation from an atomically thin semiconductor. *Nat. Phys.* **13**, 262–265 (2017).
174. Heide, C. *et al.* High-harmonic generation from artificially stacked 2D crystals. *Nanophotonics* **12**, 255–261 (2023).

175. Maroju, P. K. *et al.* Attosecond pulse shaping using a seeded free-electron laser. *Nature* **578**, 386–391 (2020).
176. Franken, P. A. & Ward, J. F. Optical harmonics and nonlinear phenomena. *Rev. Mod. Phys.* **35**, 23–39 (1963).
177. Chang, D. E., Sørensen, A. S., Demler, E. A. & Lukin, M. D. A single-photon transistor using nanoscale surface plasmons. *Nat. Phys.* **3**, 807–812 (2007).
178. Hwang, J. *et al.* A single-molecule optical transistor. *Nature* **460**, 76–80 (2009).
179. Turchette, Q. A., Hood, C. J., Lange, W., Mabuchi, H. & Kimble, H. J. Measurement of conditional phase shifts for quantum logic. *Phys. Rev. Lett.* **75**, 4710–4713 (1995).
180. Volz, T. *et al.* Ultrafast all-optical switching by single photons. *Nat. Photonics* **6**, 605–609 (2012).
181. Schuster, I. *et al.* Nonlinear spectroscopy of photons bound to one atom. *Nat. Phys.* **4**, 382–385 (2008).
182. Lounis, B. & Moerner, W. E. Single photons on demand from a single molecule at room temperature. *Nature* **407**, 491–493 (2000).
183. Castelletto, S. *et al.* A silicon carbide room-temperature single-photon source. *Nat. Mater.* **13**, 151–156 (2014).
184. Harris, S. E., Field, J. E. & Imamoglu, A. Nonlinear optical processes using electromagnetically induced transparency. *Phys. Rev. Lett.* **64**, 1107–1110 (1990).
185. Fushman, I. *et al.* Controlled phase shifts with a single quantum dot. *Science* **320**, 769–772 (2008).
186. Scuri, G. *et al.* Large excitonic reflectivity of monolayer $MoSe_2$ encapsulated in hexagonal boron nitride. *Phys. Rev. Lett.* **120**, 037402 (2018).
187. Shahnazaryan, V., Iorsh, I., Shelykh, I. A. & Kyriienko, O. Exciton-exciton interaction in transition-metal dichalcogenide monolayers. *Phys. Rev. B.* **96**, 115409 (2017).
188. Tagarelli, F. *et al.* Electrical control of hybrid exciton transport in a van der Waals heterostructure. *Nat. Photonics* **17**, 615–621 (2023).
189. Zhang, L. *et al.* Electrical control and transport of tightly bound interlayer excitons in a $MoSe_2$/hBN/$MoSe_2$ heterostructure. *Phys. Rev. Lett.* **132**, 216903 (2024).
190. Rapaport, B. L. A. Exciton correlations in coupled quantum wells and their luminescence blue shift. *Physics Review B* **80**, 195313 (2009).
191. Movva, H. C. P. *et al.* Tunable Γ-K valley populations in hole-doped trilayer WSe_2. *Phys. Rev. Lett.* **120**, 107703 (2018).
192. Uto, T. *et al.* Interaction-Induced ac Stark Shift of Exciton-Polaron Resonances. *Phys. Rev. Lett.* **132**, 056901 (2024).
193. Deng, H., Haug, H. & Yamamoto, Y. Exciton-polariton Bose-Einstein condensation. *Rev. Mod. Phys.* **82**, 1489–1537 (2010).
194. Saba, M. Intrinsic non-linearities in exciton-cavity-coupled systems. *Physica B Condens. Matter* **272**, 472–475 (1999).
195. Ciuti, C., Schwendimann, P. & Quattropani, A. Theory of polariton parametric interactions in semiconductor microcavities. *Semicond. Sci. Technol.* **18**, S279–S293 (2003).
196. G. Rochat, C. Ciuti, V. Savona, C. Piermarocchi, A. Quattropani, and P. Schwendimann. Excitonic Bloch equations for a two-dimensional system of interacting excitons. *Phys. Rev. B.* **61**, 13856–13862 (2000).
197. Stepanov, P. *et al.* Exciton-exciton interaction beyond the hydrogenic picture in a MoSe_{2} monolayer in the strong light-matter coupling regime. *Phys. Rev. Lett.* **126**, 167401 (2021).

198. Wei, K. *et al.* Charged biexciton polaritons sustaining strong nonlinearity in 2D semiconductor-based nanocavities. *Nat. Commun.* **14**, 5310 (2023).
199. Emmanuele, R. P. A. *et al.* Highly nonlinear trion-polaritons in a monolayer semiconductor. *Nat. Commun.* **11**, 3589 (2020).
200. Louca, C. *et al.* Interspecies exciton interactions lead to enhanced nonlinearity of dipolar excitons and polaritons in MoS2 homobilayers. *Nat. Commun.* **14**, 3818 (2023).
201. Wild, D. S., Shahmoon, E., Yelin, S. F. & Lukin, M. D. Quantum nonlinear optics in atomically thin materials. *Phys. Rev. Lett.* **121**, 123606 (2018).
202. Zhang, L. *et al.* Van der Waals heterostructure polaritons with moiré-induced nonlinearity. *Nature* **591**, 61–65 (2021).
203. Park, H. *et al.* Dipole ladders with large Hubbard interaction in a moiré exciton lattice. *Nat. Phys.* **19**, 1286–1292 (2023).
204. Xiong, R. *et al.* Correlated insulator of excitons in WSe_2/WS_2 moiré superlattices. *Science* **380**, 860–864 (2023).
205. Gao, B. *et al.* Excitonic Mott insulator in a Bose-Fermi-Hubbard system of moiré WS_2/WSe_2 heterobilayer. *Nat. Commun.* **15**, 2305 (2024).
206. A. Verger, C. Ciuti, and I. Carusotto. Polariton quantum blockade in a photonic dot. *Phys. Rev. B Condens. Matter Mater. Phys.* **73**, 193306 (2006).
207. Muñoz-Matutano, G. *et al.* Emergence of quantum correlations from interacting fibre-cavity polaritons. *Nature materials* vol. 18 213–218 (2019).
208. Somaschi, N. *et al.* Near-optimal single-photon sources in the solid state. *Nat. Photonics* **10**, 340–345 (2016).
209. He, Y.-M. *et al.* On-demand semiconductor single-photon source with near-unity indistinguishability. *Nat. Nanotechnol.* **8**, 213–217 (2013).
210. Delteil, A. *et al.* Towards polariton blockade of confined exciton-polaritons. *Nat. Mater.* **18**, 219–222 (2019).
211. Moody, G., Chang, L., Steiner, T. J. & Bowers, J. E. Chip-scale nonlinear photonics for quantum light generation. *AVS Quantum Sci.* **2**, 041702 (2020).
212. Elshaari, A. W., Pernice, W., Srinivasan, K., Benson, O. & Zwiller, V. Hybrid integrated quantum photonic circuits. *Nat. Photonics* **14**, 285–298 (2020).
213. Sirleto, L. & Righini, G. An introduction to nonlinear integrated photonics: Structures and devices. *Micromachines* **14**, 614 (2023).
214. Bogdanov, A. A., Makarov, S. & Kivshar, Y. New frontiers in nonlinear nanophotonics. *Nanophotonics* **13**, 3175–3179 (2024).
215. Perea-Causín, R. *et al.* Exciton optics, dynamics, and transport in atomically thin semiconductors. *APL Mater.* **10**, 100701 (2022).
216. Li, W., Brumme, T. & Heine, T. Relaxation effects in transition metal dichalcogenide bilayer heterostructures. *Npj 2D Mater. Appl.* **8**, 1–11 (2024).
217. Guo, Q. *et al.* Efficient frequency mixing of guided surface waves by atomically thin nonlinear crystals. *Nano Lett.* **20**, 7956–7963 (2020).
218. Huang, D., Choi, J., Shih, C.-K. & Li, X. Excitons in semiconductor moiré superlattices. *Nat. Nanotechnol.* **17**, 227–238 (2022).
219. Yang, X., Wang, X., Faizan, M., He, X. & Zhang, L. Second-harmonic generation in 2D moiré superlattices composed of bilayer transition metal dichalcogenides. *Nanoscale* **16**, 2913–2922 (2024).

220. Camacho-Guardian, A. & Cooper, N. R. Moiré-induced optical nonlinearities: Single- and multiphoton resonances. *Phys. Rev. Lett.* **128**, 207401 (2022).
221. Mennel, L., Paur, M. & Mueller, T. Second harmonic generation in strained transition metal dichalcogenide monolayers: MoS_2, $MoSe_2$, WS_2, and WSe_2. *APL Photonics* **4**, 034404 (2019).
222. Khestanova, E. *et al.* Electrostatic control of nonlinear photonic-crystal polaritons in a monolayer semiconductor. *Nano Lett.* **24**, 7350–7357 (2024).
223. Moody, G., Schaibley, J. & Xu, X. Exciton dynamics in monolayer transition metal dichalcogenides. *J. Opt. Soc. Am. B* **33**, C39–C49 (2016).
224. Esmaeil Zadeh, I. *et al.* Efficient Single-Photon Detection with 7.7 ps Time Resolution for Photon-Correlation Measurements. *ACS Photonics* **7**, 1780–1787 (2020).
225. Korzh, B. *et al.* Demonstration of sub-3 ps temporal resolution with a superconducting nanowire single-photon detector. *Nat. Photonics* **14**, 250–255 (2020).
226. Choudhury, T. H., Zhang, X., Al Balushi, Z. Y., Chubarov, M. & Redwing, J. M. Epitaxial Growth of Two-Dimensional Layered Transition Metal Dichalcogenides. *Annu. Rev. Mater. Res.* **50**, 155–177 (2020).
227. Zhang, T., Wang, J., Wu, P., Lu, A.-Y. & Kong, J. Vapour-phase deposition of two-dimensional layered chalcogenides. *Nat. Rev. Mater.* **8**, 799–821 (2023).
228. Kim, J.-Y., Ju, X., Ang, K.-W. & Chi, D. Van der Waals layer transfer of 2D materials for monolithic 3D electronic system integration: Review and outlook. *ACS Nano* **17**, 1831–1844 (2023).
229. Li, H. *et al.* Imaging moiré flat bands in three-dimensional reconstructed WSe_2/WS_2 superlattices. *Nat. Mater.* **20**, 945–950 (2021).
230. Zhang, Y. *et al.* Atom-by-atom imaging of moiré transformations in 2D transition metal dichalcogenides. *Sci. Adv.* **10**, eadk1874 (2024).
231. Frisenda, R. *et al.* Recent progress in the assembly of nanodevices and van der Waals heterostructures by deterministic placement of 2D materials. *Chem. Soc. Rev.* **47**, 53–68 (2018).

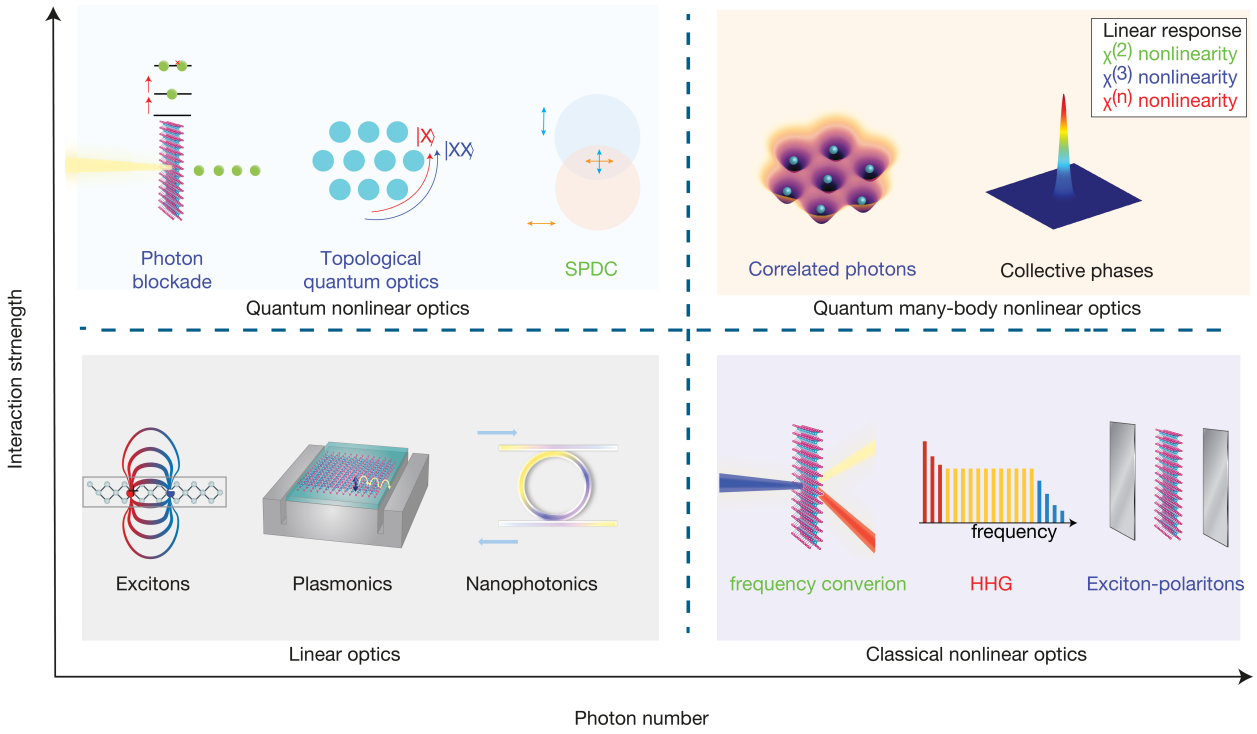

Figure 1. Nonlinear optical phenomena in different regimes. We can classify the many emerging optical phenomena in terms of the interaction strength among photons and the photon number (light intensity). The lower left vertical panel represents the classical linear optics regime, with a low number of optical excitations that are weakly interacting. Examples include excitons, plasmons, and nanophotonic devices. With an increasing number of photons, the nonlinear optical response becomes strong, leading to classical nonlinear optical phenomena, such as frequency conversion. Exciton-polaritons form when embedding excitons inside a cavity, which enhances their interactions and features intriguing properties such as condensates at high photon numbers. An interesting regime emerges in the upper left corner, where the interaction strength is so large that nonlinear effects become obvious at the few-photon regime. Examples of such include photon blockade, topological quantum systems, and entangled photon pair generation via spontaneous parametric down-conversion (SPDC). Finally, for strong interactions and large photon numbers, the system behaves as quantum many-body systems with emergent properties, including correlated Bosonic lattices and quantum fluids, which remain largely unexplored.

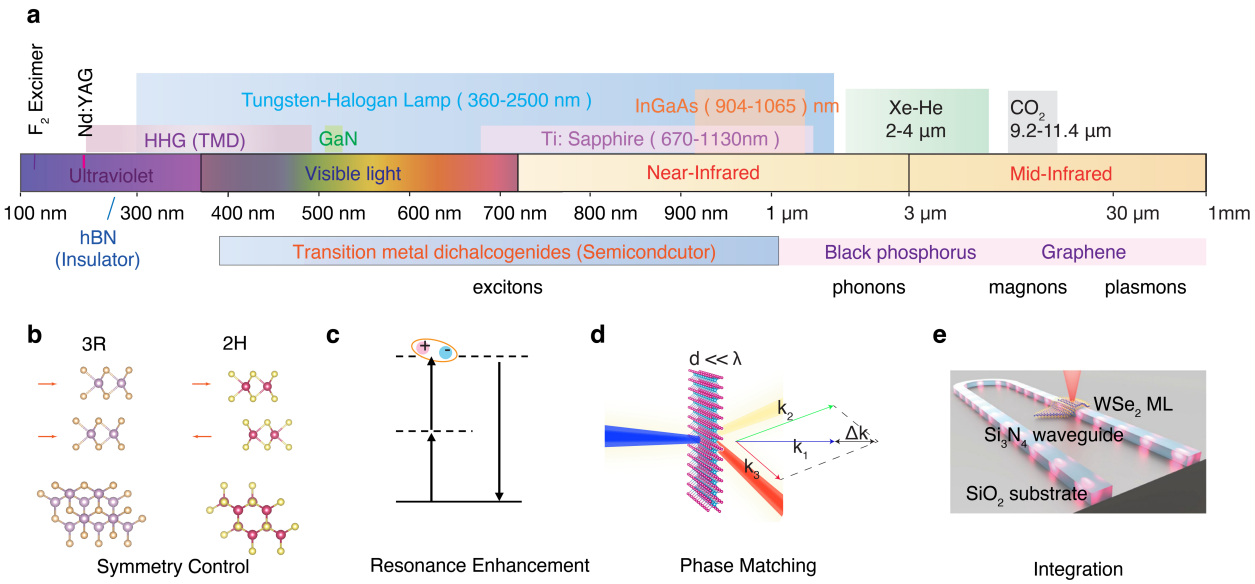

Figure 2. **a,** Electromagnetic spectrum from UV to MIR with the common light source. 2D materials offer distinct electronic and optical properties, covering a wide range of the spectrum. They also feature various optical excitations, such as excitons and magnons, which can be used to enhance nonlinear response resonantly. **b,** Control of lattice symmetry in 2D heterostructures by controlling the stacking between different layers. **c,** Enhancement of nonlinear optical response via resonance effect such as excitons. **d,** Relaxed phase matching conditions due to small propagation length. **e**, Integrating 2D materials onto photonic structures such as waveguides. **e**, Reproduced with permission from[53]. Copyright 2021 American Chemical Society.

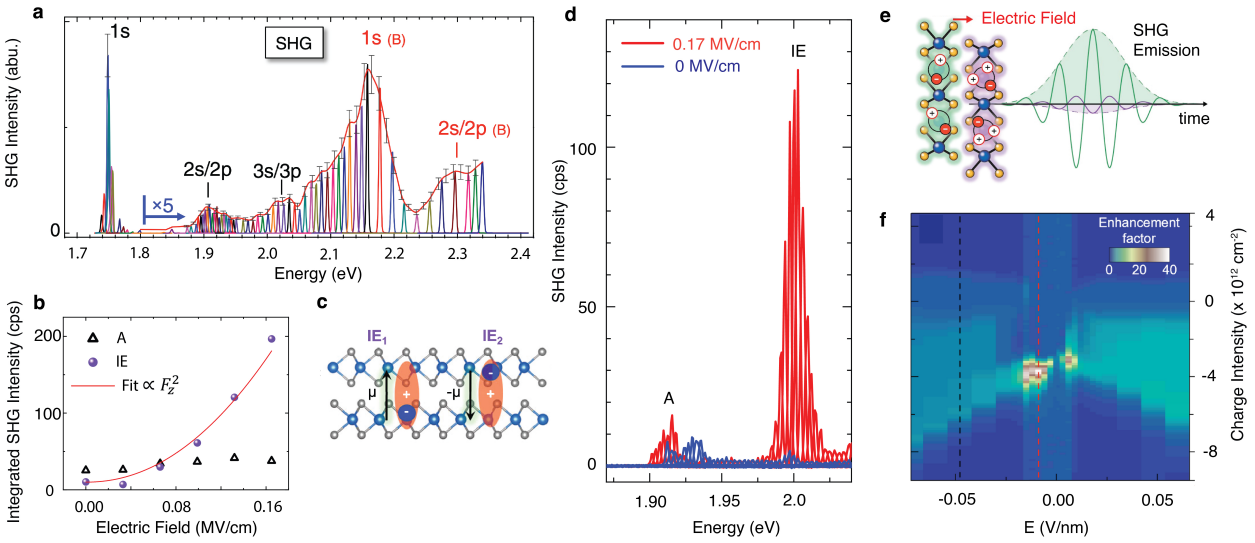

Figure 3. Exciton resonance enhancement of the SHG intensity with electrical tunability. **a**, Monolayer WSe_2 SHG spectroscopy at T = 4 K. SHG signal exhibits significant enhancement when the $2\hbar\omega$ is resonant at the exciton frequency. **b-d**, Tuning SHG signal of interlayer exciton (IE) in MoS_2 bilayer via applied electric field. **b**, The SHG amplitude (IE) shows a quadratic increase as the electric field, which breaks the inversion symmetry in natural 2H bilayer. **c**, schematic of the interlayer excitons in bilayer MoS_2. **d**, SHG spectra of A and IE exciton resonance at $F_Z = 0$ MV/cm and $F_Z = 0.17$ MV/cm. The SHG signal at $F_Z = 0.17$ MV/cm increases by a factor of 25 compared to that at zero electric field. This enhancement is due to the stark shift of the IE with the static field. At $F_Z = 0.17$ MV/cm, IE splits into two energy IE_1 and IE_2, which both contribute to the SHG signal. **e**, Schematic of the broken symmetry in bilayer WSe2 under certain doping with electric field induce SHG signal enhancement. **f**, SHG enhancement 2D map with changes of electric field and doping level. Under certain electric filed and doping, the SHG enhancement reach the maximum factor of 40. **a**, Reproduced with permission[80]. Copyright 2015, American Physical Society. **b-d**, Reproduced with permission[111]. Copyright 2021 Springer Nature Ltd. **e-f**, Reproduced with permission[114]. Copyright 2024 CC BY 4.0.

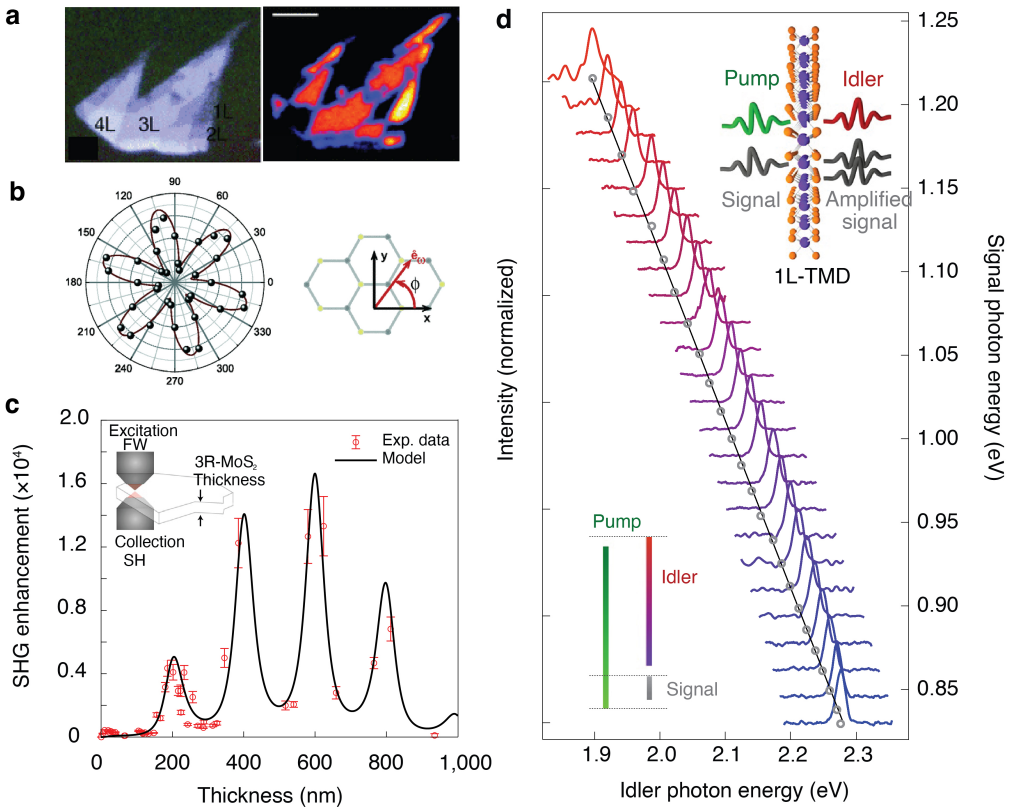

Figure 4. Second Order Nonlinearity in 2D materials. a, left panel: optical image of multilayer 2H MoS2 on quartz substrate. Right panel: SHG image for the same flake under pumping wavelength of 860nm. Due to the inversion symmetry, odd and even layer exhibits different SHG intensity contrast. **b**. left panel: Monolayer MoS_2 polar plot of the second-harmonic intensity as a function of the sample angle. Right panel: top view of the MoS_2 crystallographic orientation. Red arrow refers to the excitation laser polarization. **c**, Measured SHG enhancement of the 3R-MoS2 compared to the monolayer MoS_2 with the change of the thickness. Under the pump photon energy of 0.815 eV, the coherence length L_c is around 530nm, with the transmittance period of 182 nm. **d**, Monolayer TMD as broadband tunable OPA: the normalized tunable idler spectra measured on monolayer MoSe2 in a broad photon energy range from 1.90 eV to 2.28 eV. The spectral window is limited by the tunability of the signal beam used in the paper. **a**, **b,** Reproduced with permission from[105] . Copyright 2013, American Physical Society. **c**, Reproduced with permission from[93]. Copyright 2022 Springer Nature Ltd. **d**, Reproduced with permission from[128]. Copyright 2021 Springer Nature Ltd.

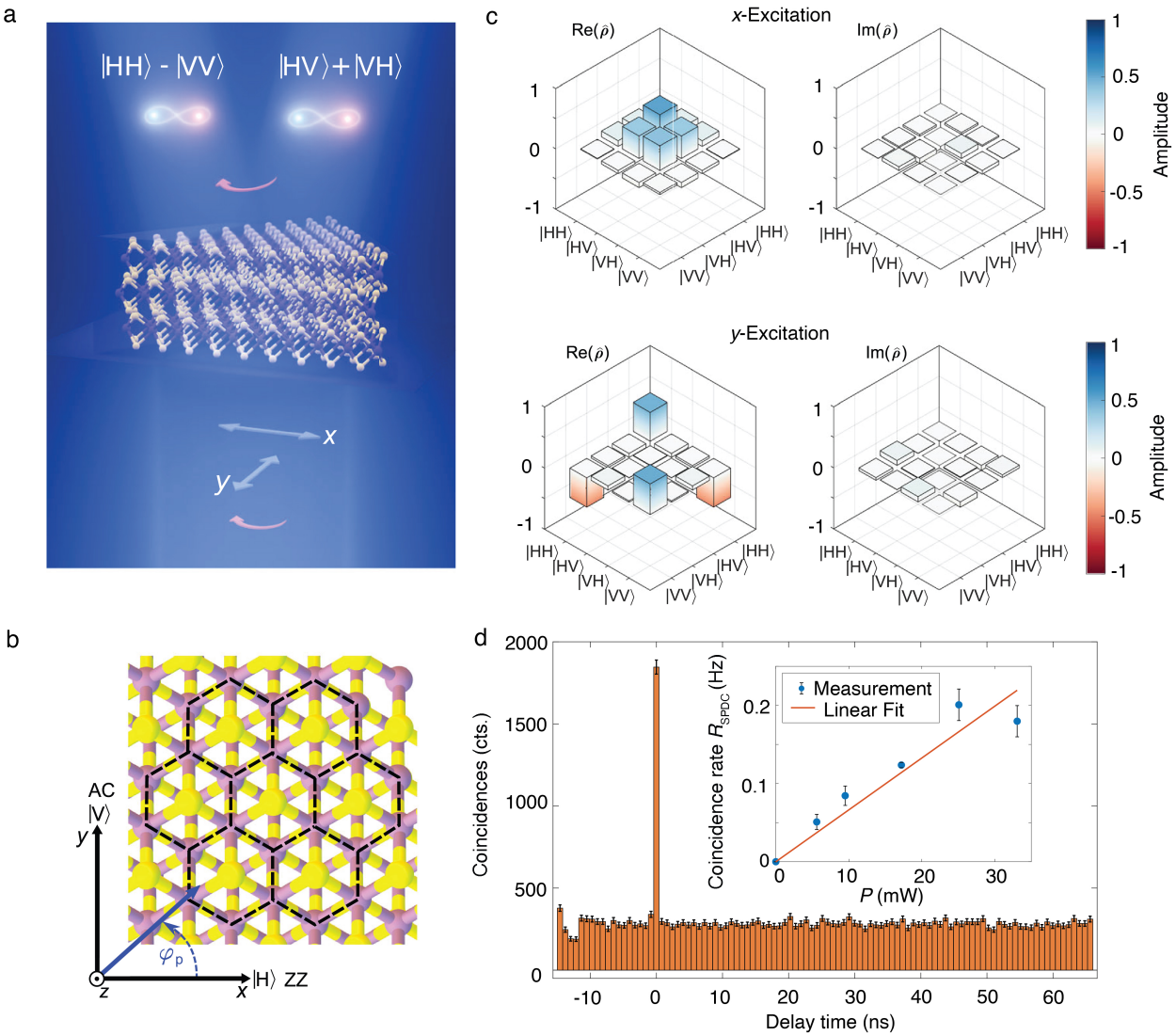

Figure 5. Generation of entangled photon pairs through SPDC. **a**, Schematic of generation pairs of polarization-entangled signal and idler photons via SPDC process in a 3R-stacked MoS_2. Different maximally entangled Bell states are generated by changing the excitation polarization. **b**, Top view of the 3R MoS_2 stack crystalline structure. The x and y direction (also refers to |H> and |V> polarization direction) are aligned with zigzag (ZZ) and armchair (AC) direction in the crystal structure. The blue arrow defines the pump polarization with the angle φ_p. **c**, Measured density matrix $\hat{\rho}$ of polarization quantum state for x and y pump direction. For both x and y linear polarizations, different maximally entangled states can be generated. **d**, Coincidence characterization of the generated photon pairs. From this one can extract the parameter, the coincidence-to-accidental ratio (CAR), which is defined as $CAR = \frac{R_{SPDC}}{R_C}$, with R_{SPDC} refers to SPDC rate and is corrected as $R_{SPDC} = R_C - R_{acc}$. R_{acc} is accidental coincidence counting. As photons generated by different SPDC process happen to arrive at the detector at the same time can contribute to the $g^2(0)$ counts, but this cannot be attributed to correlated photon. CAR in this frame is 5.5 at $P = 17$ mW. **a-d**, Reproduced with permission[137]. Copyright 2024 Springer Nature Ltd.

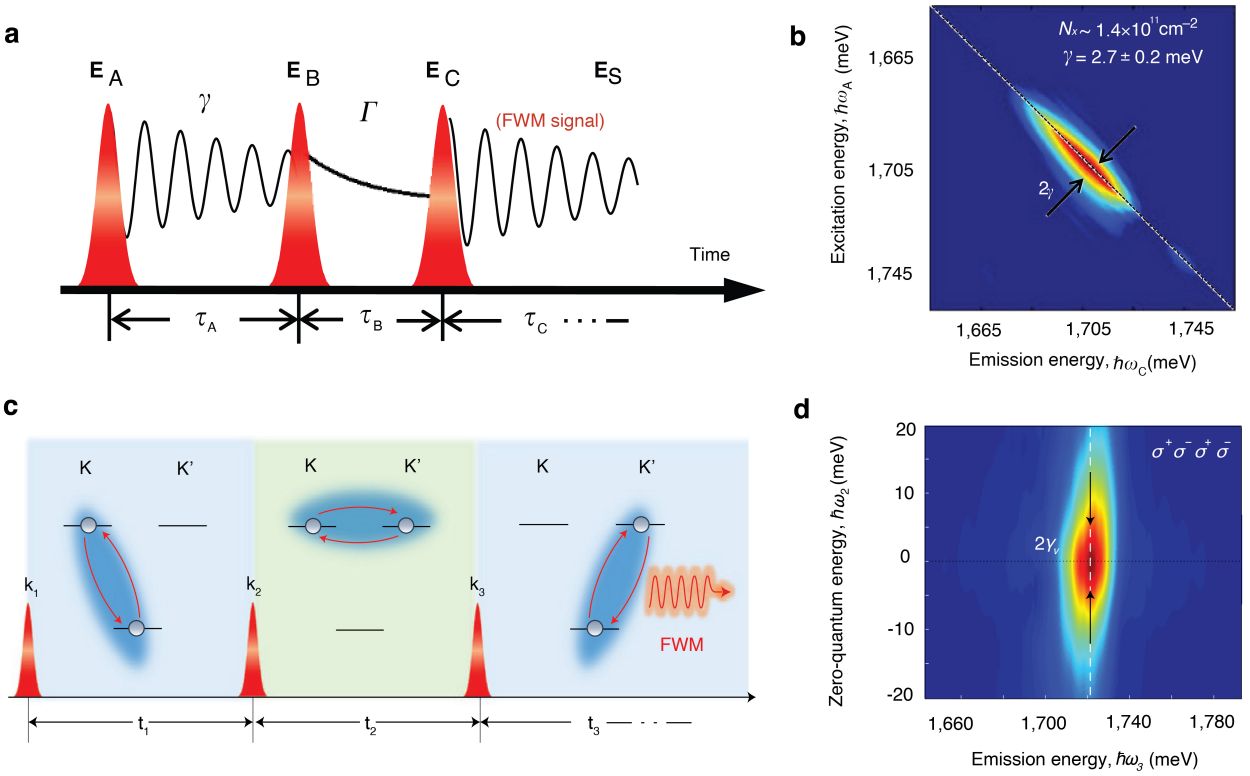

Figure 6. Examples of Two-dimensional coherent spectroscopy utilizing four-wave mixing. **a,** Schematic of the 2D coherent spectroscopy technique. Three phase-stabilized pulses radiate on the sample and then emit the FWM signal with the sequence shown in the figure. Scanning τ_A with τ_B fixed explore the coherent nature (γ) for excitons in TMD, while scan τ_B with τ_A fixed explore the population relaxation Γ.**b**, 2D Fourier-transform spectra of the echo signal reveling the linewidth broadening mechanism. The intrinsic homogeneous linewidth of the exciton resonance corresponds to the cross-diagonal line (dashed line), while the total linewidth includes inhomogeneous broadening. The exciton dephasing rate γ can be extrapolated from the linewidth. **c-d**, Detection of valley coherence in monolayer TMD. **c,** As the first and third pulses are co-polarized (σ^+) and the second and detected polarization are co-polarized but with opposite helicity (σ-), the first pulse (σ^+)creates exciton population in K valley with a decay rate of Γ_k. The second pulse (σ-) creates a coherent superposition between K and K' valleys with a coherent decay rate of γ_v. The third pulse then converts the non-radiative valley coherence to optical coherence in K' valley between the exciton and ground state. **d,** 2D spectrum using alternative helicity of the excitation and collection pulses. As the delay t_1 is fixed and t_2 is swept, the zero-quantum energy $\hbar\omega_2$ is given during t_2 by Fourier transform. The width of the line shape along $\hbar\omega_3$ demonstrate the measured valley coherence decay rate of $\gamma_v = 6.9 \pm 0.2$ meV. **a,b**, Reproduced with permission[152]. Copyright 2015 Springer Nature Ltd. **c,d,** Reproduced with permission[156]. Copyright 2016 Springer Nature Ltd.

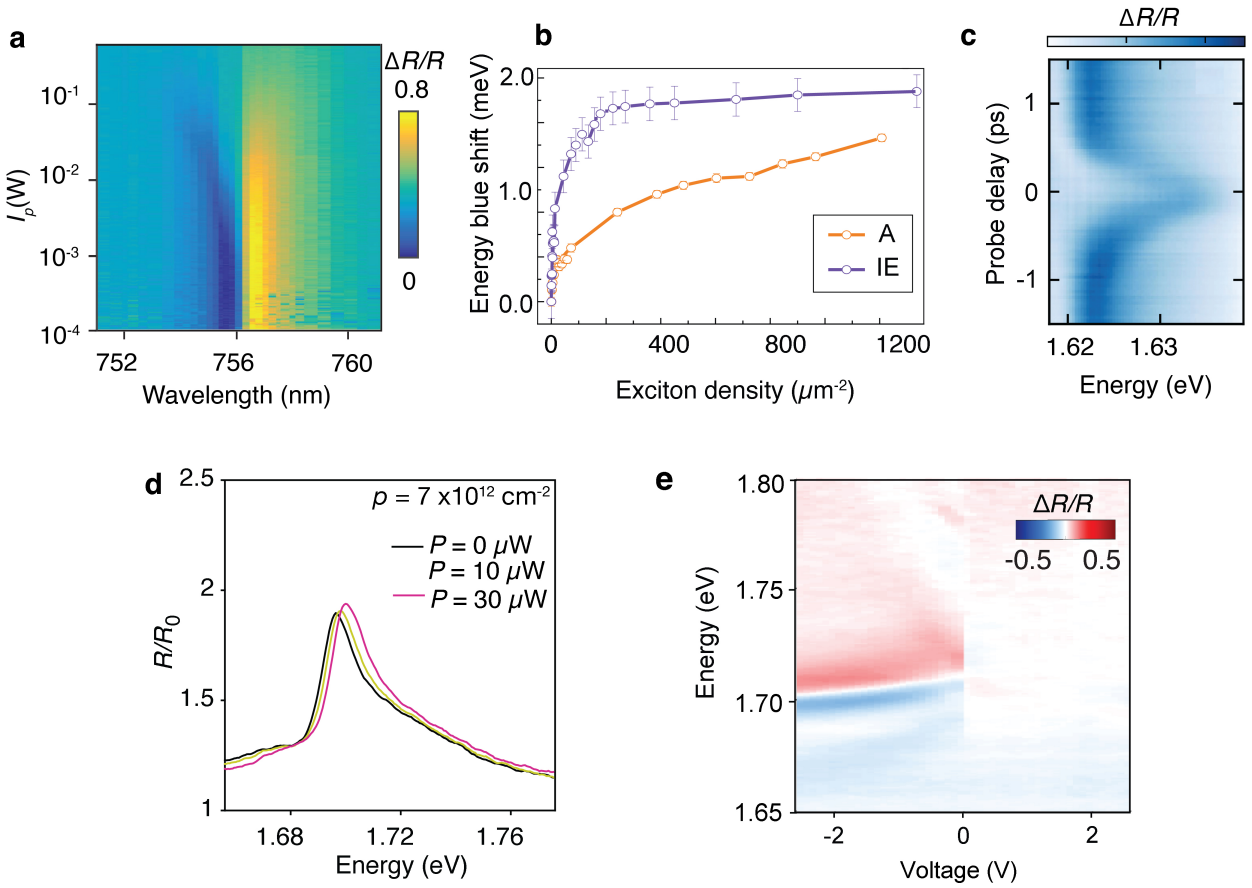

Figure 7. Exciton and polaron optical nonlinearity in TMD. a, Reflectance of monolayer $MoSe_2$ as a function of the peak laser power at different excitation wavelength at 4K. **b**, Intralayer(A) and interlayer (IE) Exciton reflection relative energy blueshift with increasing exciton density in homobilayer MoS_2. **c**, AC stark shift of the attractive polaron in monolayer $MoSe_2$ as a function of the pump-probe delay time under pump laser peak power of 2 GW/cm^2. **d**, Trilayer WSe_2 Fermi-polaron reflectance contrast as a function of the CW (635nm) laser excitation power. **e**, Relative change in the reflectance induced by CW laser pumping under different doping. The nonlinearity of Fermi polaron only shows up at the hole-doped regime (negative voltage) due to the valley polarization in trilayer WSe_2. **a**, Reproduced with permission[186]. Copyright 2018 American Physical Society. **b**, Reproduced with permission[47]. Copyright 2022 Springer Nature Ltd. **c**, Reproduced with permission[192]. Copyright 2024 American Physical Society. **d,e**, Reproduced with permission[46]. Copyright 2024 Springer Nature Ltd.

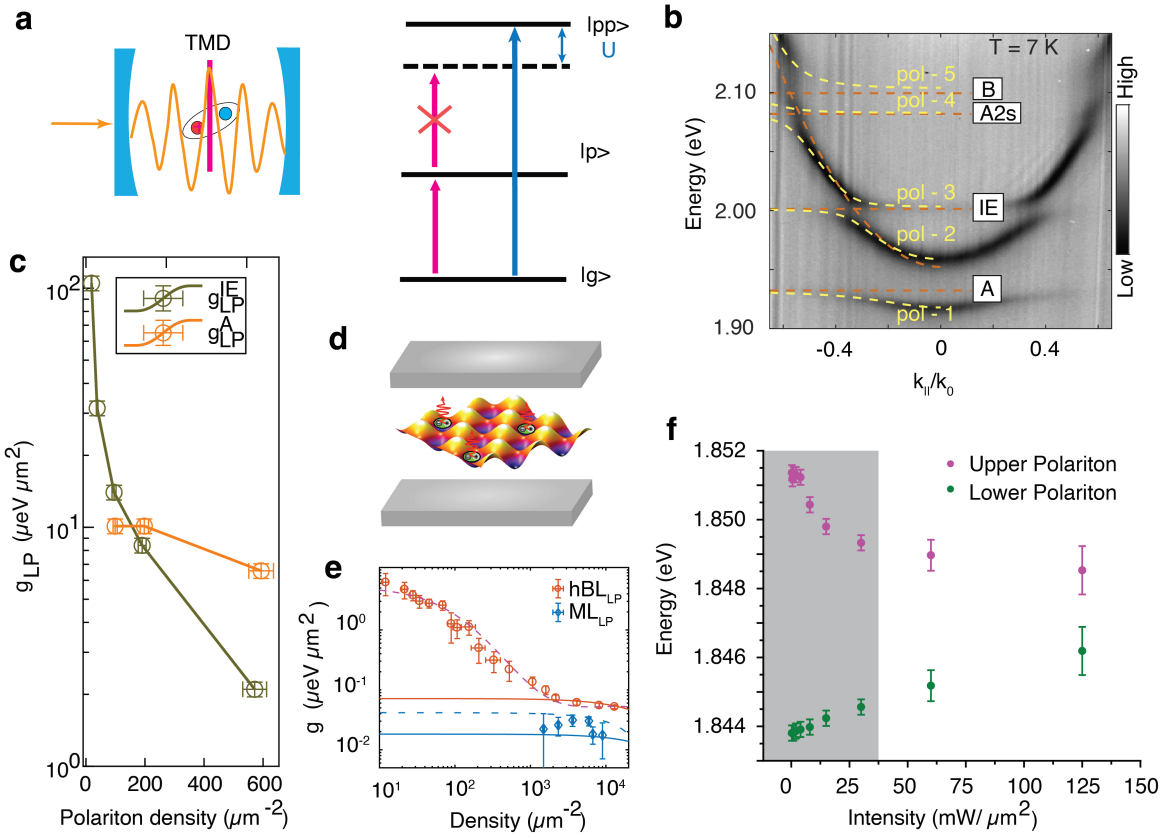

Figure 8. Nonlinearity enhancement via exciton polariton formation in cavity. a, Schematic of polariton blockade spectrum happened in cavity. Due to the strong interaction strength U between polaritons (U is larger than the polariton linewidth), two polariton states blueshift, the photon which excite the system from ground to the one-polariton state cannot excite the 2nd polariton anymore due to the addition energy requirement. **b,** Differential reflection at T =7K showing the polariton branches formed by intralayer (A, A 2S, B) and interlayer (IE) exciton coupled to the cavity mode in bilayer MoS_2 embedded into microcavity. Strong coupling between the exciton state and cavity mode can be demonstrated by the anti-crossing behavior between each branch. **c**, Nonlinear interaction strength of A and Interlayer exciton as a function of the polariton density. At low polariton density, dipolar polariton owns larger interaction strength due to dipole-dipole repulsion. **d-e**, Moiré polariton system: **d**, Excitons confined in Moiré superlattice and then coupled with cavity photon forms Moiré polariton, which exhibit large nonlinearity due to the exciton blockade. **e**, Nonlinear interaction strength of moiré lower polariton (orange) and intralayer exciton polariton(blue) as a function of polariton density. **f**, Nonlinearity for 2S polariton. The coupling strength reduces with increasing excitation power density due to the phase space filling. **b, c**, Reproduced with permission[47]. Copyright 2022 Springer Nature Ltd. **d,e**, Reproduced with permission[202], Copyright 2022 Springer Nature Ltd. **f**, Reproduced with permission[48]. Copyright 2021 Springer Nature Ltd.